Department of Applied Physics

Spatially resolved rheology modeling of complex fluids

Mikael Mohtaschemi

Aalto University

DOCTORAL DISSERTATIONS

Aalto University publication series
DOCTORAL DISSERTATIONS 152/2015

Spatially resolved rheology modeling of complex fluids

Mikael Mohtaschemi

A doctoral dissertation completed for the degree of Doctor of Science (Technology) to be defended, with the permission of the Aalto University School of Science, at a public examination held at the lecture hall A123 of the school on 2 November 2015 at 12.

Aalto University
School of Science
Department of Applied Physics
Complex Systems and Materials

Supervising professor
Professor Mikko Alava, Aalto University, Finland

Thesis advisor
D.Sc. (Tech.) Antti Puisto, Aalto University, Finland

Preliminary examiners
Professor Luca Brandt, KTH, Sweden
Professor Jari P.I. Hämäläinen, LUT, Finland

Opponent
Professor Federico Toschi, TU/e, Netherlands

Aalto University publication series
DOCTORAL DISSERTATIONS 152/2015

ISBN 978-952-60-6419-2 (printed)
ISBN 978-952-60-6420-8 (pdf)
ISSN-L 1799-4934
ISSN 1799-4934 (printed)
ISSN 1799-4942 (pdf)
http://urn.fi/URN:ISBN:978-952-60-6420-8

Unigrafia Oy
Helsinki 2015

Finland

441 697
Printed matter

Aalto University

Abstract

Aalto University, P.O. Box 11000, FI-00076 Aalto www.aalto.fi

Author
Mikael Mohtaschemi

Name of the doctoral dissertation
Spatially resolved rheology modeling of complex fluids

Publisher School of Science

Unit Department of Applied Physics

Series Aalto University publication series DOCTORAL DISSERTATIONS 152/2015

Field of research Theoretical and Computational Physics

Manuscript submitted 15 June 2015 **Date of the defence** 2 November 2015

Permission to publish granted (date) 26 August 2015 **Language** English

☐ **Monograph** ☒ **Article dissertation (summary + original articles)**

Abstract

Many complex fluids show yield stress behavior. However, the term yield stress has been subject of much controversy. The separation of yield stress fluids into thixotropic and simple ones resolves many of these issues. This division is mainly driven by experimental results and is suspect to active theoretical development.

This thesis addresses yield stress fluids and associated phenomena through continuum modeling for fluids with time dependent structure evolution. In addition to homogeneous laminar shear modeling, the emergence of spatial effects in viscometric flow situations is addressed. Therefore the models are coupled to the creeping flow solution (1-D Stokes equation) of a concentric cylinder geometry, which enables comparisons with experimental observations.

Further, the results from thixotropic yield stress fluids are applied to the analysis of rheology measurements of nanocellulose suspensions, which have peculiar rheological properties. In particular, shear rate sweeps are simulated utilizing a structural model for thixotropic yield stress fluids. The results indicate that spatial flow heterogeneities have to be taken into account. Additionally wall slip, which is known to play an important role in the flow of complex fluids is addressed through a simple model. The results in this thesis add to the understanding of nanocellulose suspensions and complex fluids in general.

Keywords rheology modeling, yield stress, complex fluids, nanocellulose suspensions

ISBN (printed) 978-952-60-6419-2 **ISBN (pdf)** 978-952-60-6420-8

ISSN-L 1799-4934 **ISSN (printed)** 1799-4934 **ISSN (pdf)** 1799-4942

Location of publisher Helsinki **Location of printing** Helsinki **Year** 2015

Pages 131 **urn** http://urn.fi/URN:ISBN:978-952-60-6420-8

Aalto-yliopisto

Tiivistelmä

Aalto-yliopisto, PL 11000, 00076 Aalto www.aalto.fi

Tekijä
Mikael Mohtaschemi

Väitöskirjan nimi
Kompleksisten nesteiden spatiaalinen reologiamallinnus

Julkaisija Perustieteiden korkeakoulu

Yksikkö Teknillisen fysiikan laitos

Sarja Aalto University publication series DOCTORAL DISSERTATIONS 152/2015

Tutkimusala Teoreettinen ja laskennallinen fysiikka

Käsikirjoituksen pvm 15.06.2015 **Väitöspäivä** 02.11.2015

Julkaisuluvan myöntämispäivä 26.08.2015 **Kieli** Englanti

☐ **Monografia** ☒ **Yhdistelmäväitöskirja (yhteenveto-osa + erillisartikkelit)**

Tiivistelmä

Vaikka monilla kompleksisilla nesteillä on tunnetusti myötöraja, kyseiseen käsitteeseen ja sen määrittelyyn on kuitenkin liittynyt paljon ristiriitoja. Jakamalla myötörajanesteet yksinkertaisiin sekä tiksotrooppisiin, monet käsitteelliset ongelmat poistuvat. Tämä jako on toistaiseksi pitkälti kokeellisten tulosten varassa ja siihen liittyvä teoria on aktiivisen kehityksen alla.

Tämä väitöskirja käsittelee myötörajaa ja siihen liittyviä ilmiöitä jatkumotason malleilla sellaisille nesteille, joilla on ajassa kehittyvä rakenne. Homogeenisen, laminaarisen leikkausvirtauksen lisäksi käsitellään spatiaalisten ilmiöiden syntyä. Tätä varten mallit yhdistetään sylinteri-sylinteri geometrian yksiulotteisen Stokesin virtauksen ratkaisuun mahdollistaen samalla vertailun kokeellisten havaintojen kanssa.

Tiksotrooppisten myötörajanesteiden tuloksia sovelletaan nanoselluloosasuspensioden reologian analysointiin. Näiden suspensioden kokeellisia leikkausvirtauspyyhkäisyjä simuloidaan tiksotrooppisella rakennemallilla. Tulosten perusteella virtauksen geometrisiä epähomogenisuuksia on otettava huomioon. Lisäksi kokeellisesti tärkeäksi havaittua liusumisilmiöta (wall slip), käsitellään yksinkertaisen mallin avulla. Tämän väitöskirjan tulokset edistävät nanoselluloosasuspensioden sekä yleisesti kompleksisten nesteiden ymmärrystä.

Avainsanat reologiamallinnus, myötöraja, kompleksiset nesteet, nanoselluloosasuspensiot

ISBN (painettu) 978-952-60-6419-2 **ISBN (pdf)** 978-952-60-6420-8

ISSN-L 1799-4934 **ISSN (painettu)** 1799-4934 **ISSN (pdf)** 1799-4942

Julkaisupaikka Helsinki **Painopaikka** Helsinki **Vuosi** 2015

Sivumäärä 131 **urn** http://urn.fi/URN:ISBN:978-952-60-6420-8

Preface

The research work in this thesis has been performed in the Complex Systems and Materials (CSM) Group of the Department of Applied Physics at the Aalto University School of Science.

First of all I want to thank my instructor Antti Puisto for the excellent support during this thesis. On the same note, I want to thank Mikko Alava for the supervision and the fact that I was privileged to be part of his group.

Collaboration is a cornerstone of science. I would like to express my gratitude to my co-authors Antti Puisto, Xavier Illa, Marko Korhonen, Mikko Alava, Anni Karppinen, Jukka Seppälä, Markus Nuopponen, Katarina Dimic-Misic, Thaddeus Maloney, and Jouni Paltakari. Many thanks to the pre-examiners Jari Hämäläinen, Luca Brandt and the opponent Federico Toschi for evaluating the thesis.

I thank my fellow CSM group members as well as many other colleagues with whom I have had the pleasure to discuss ideas and thoughts about science and various other aspects of life. I was privileged to guide the hard working undergraduate students Marko Korhonen and Henri Salmenjoki.

I want to thank the administrative as well as the facilities stuff at our department. I would also like to acknowledge financial support from the Academy of Finland within the framework of the International Doctoral Programme in Bioproducts Technology (PaPSaT) and through its Centres of Excellence Programme (2012-2017) under Project No. 251748. The calculations presented in this thesis were performed using computer resources within the Aalto University School of Science "Science-IT" project.

I want to thank my friends and family, who have helped in many ways. Finally, my thanks and utmost appreciation goes to my amazing wife Riikka and our awesome kids Kevin, Edith, and Edwin for their support.

Espoo, September 30, 2015,

Mikael Mohtaschemi

Contents

List of Publications

This thesis consists of an overview and of the following publications which are referred to in the text by their Roman numerals.

I Mikael Mohtaschemi, Antti Puisto, Xavier Illa, and Mikko J. Alava. Rheology dynamics of aggregating colloidal suspensions. *Soft Matter*, **10** 2971–2981, January 2014.

II Antti Puisto, Mikael Mohtaschemi, Xavier Illa, and Mikko J. Alava. Dynamic hysteresis in the rheology of complex fluids. *Physical Review E*, **91** 042314, April 2015.

III Mikael Mohtaschemi, Katarina Dimic-Misic, Antti Puisto, Marko Korhonen, Thaddeus Maloney, Jouni Paltakari, and Mikko J. Alava. Rheological characterization of fibrillated cellulose suspensions via bucket vane viscometer. *Cellulose*, **21** 1305–1312 , March 2014.

IV Mikael Mohtaschemi, Anni Sorvari, Antti Puisto, Markus Nuopponen, Jukka Seppälä, and Mikko J. Alava. The vane method and kinetic modeling: shear rheology of nanofibrillated cellulose suspensions. *Cellulose*, **21** 3913–3925, August 2014.

V Marko Korhonen, Mikael Mohtaschemi, Antti Puisto, Xavier Illa, and Mikko J. Alava. Apparent wall slip in non-Brownian hard sphere suspensions . *The European Physical Journal E*, **38** 46, May 2015.

Author's Contribution

Publication I: "Rheology dynamics of aggregating colloidal suspensions"

The author participated in writing the code, did all the simulations and wrote the first version of the draft.

Publication II: "Dynamic hysteresis in the rheology of complex fluids"

The author was actively involved in specifying and interpreting the numerical simulations and writing the paper

Publication III: "Rheological characterization of fibrillated cellulose suspensions via bucket vane viscometer"

The author did the numerical part of the paper, prepared the figures and was actively involved in writing the paper

Publication IV: "The vane method and kinetic modeling: shear rheology of nanofibrillated cellulose suspensions"

The author developed and implemented the model, did all the simulations and was actively involved in writing the paper

Publication V: "Apparent wall slip in non-Brownian hard sphere suspensions "

The author was actively involved in the model development and numerical implementation, and writing the paper

1. Introduction

The term *rheo* means to flow in Greek. Thus, originally rheology was understood as the study of flow. However, the distinction between flowing and not flowing is often difficult to make. For example, in the famous pitch drop experiment the formation of a single droplet takes of the order of 10 years [1]. Nowadays, rheology deals with the study of stresses of materials under deformation. The emphasis is here mainly on complex fluids – materials in between solids and ideal fluids.

Complex fluids can be found almost anywhere: Paints and cosmetics can be easily applied and yet do not drip off thanks to their rheological properties. In these products the request to *stir* or *shake well before use* can, in certain cases, be made obsolete by tuning the rheological properties. In the construction industry rheology plays an important role since the properties of fresh concrete have to meet certain criteria [2]. Likewise, understanding the rheology of waxy crude oils is important in the oil industry [3]. As these few examples demonstrate, being able to understand and tailor the rheological behavior of complex fluids is clearly of great relevance.

Nanocellulose water suspensions are complex fluids with peculiar properties [4]. Already at very low concentrations nanocellulose modifies the fluid properties heavily [5]. The rheology of nanocellulose suspensions is currently under active study, and it is relevant in various potential applications [6, 7, 8, 9].

Not too long ago the term thixotropy, related to time dependency of a fluid, could lead to great controversy as it was used to describe different things [10, 11, 12]. Similar problems are related to the property termed yield stress. Classically for stresses below the yield stress a material behaves like a solid and like a fluid above it. The question of whether there is actually a real solid behavior below the yield stress has been subject to

a lot of debate [13, 14]. Another problem is related to the fact that the yield stress is not necessarily unique – it can depend on the measurement procedure [15]. It was then suggested that yield stress fluids should be divided into simple and thixotropic ones which would resolve most of the issues [16, 17]. Hereby the thixotropic yield stress fluids show time dependence, while for the simple yield stress fluids the time dependence could be normally neglected. Further, in the thixotropic yield stress fluids the existence of a critical shear rate results in heterogeneous flows and viscosity bifurcation [16, 18]. However, also in simple yield stress fluids heterogeneous flows, in terms of transient shear banding were observed [19, 20]. The issue is further complicated by the fact that additional effects, most importantly wall slip, have to be considered simultaneously [21]. Much work remains to be done both theoretically and experimentally [22, 23].

The topic of this thesis is rheology modeling at the continuum scale. In particular yield stress fluids and flow heterogeneities arising in these are addressed. Publication I studies the simple shear rheology of aggregating colloidal systems, such as the influence of the initial state, transient and steady state shear banding through a model based on population balance equations (PBE). In Publication II the focus lies on a more complex measurement protocol, namely shear rate sweep experiments, which are frequently utilized to measure steady state flow curves. There a structural model is employed to gain insight into the hysteresis observed in simple yield stress fluids during these sweep measurements. In Publication III and IV, the results of Publication I and II were applied to measure and model the rheology of nanocellulose suspensions. In Publication V a simple model for wall slip is studied.

The rest of this thesis is organized as follows: Chapter 2 introduces the theoretical background, and the methods and models utilized in the publications. In Chapter 3 the main results of the publications are highlighted and discussed. Finally, in Chapter 4 a concluding summary is given.

2. Theoretical background

In this part the theoretical background of the thesis is summarized in short. References to more detailed background information are also given.

2.1 Rheology

For continuous media it is convenient to rewrite Newton's second law (conservation of momentum) in terms of density instead of mass. In Cartesian coordinates, the stress tensor is given by

$$\underline{\underline{\sigma}} = \begin{bmatrix} \sigma_{x,x} & \sigma_{x,y} & \sigma_{x,z} \\ \sigma_{y,x} & \sigma_{y,y} & \sigma_{y,z} \\ \sigma_{z,x} & \sigma_{z,y} & \sigma_{z,z} \end{bmatrix} \tag{2.1}$$

The momentum balance is then

$$\rho \frac{D\underline{v}}{Dt} = \nabla \cdot \underline{\underline{\sigma}} + \rho \underline{g}, \tag{2.2}$$

where $\underline{v}$ is the velocity, t the time, and ρ is the density. In the last term $\underline{g}$ represents body forces per unit mass (e.g. gravity). The stress can be decomposed into

$$\underline{\underline{\sigma}} = p\underline{\underline{I}} + \underline{\underline{\tau}}, \tag{2.3}$$

where p is the thermodynamic pressure, and I the unit identity vector and $\underline{\underline{\tau}}$ the extra stress tensor. The crucial question is then: How is the extra stress tensor $\underline{\underline{\tau}}$ related to the deformation (and its history) for a given material? The model describing this relationship is termed the stress constitutive equation. Obtaining this relationship is one of the main objectives in rheology. [24]

The prime example of a constitutive equation was described by Newton in 1687 in the *Philosophie Principia Mathematica*: "The resistance which arises from the lack of slipperiness of the parts of the liquid, other things

being equal, is proportional to the velocity with which the parts of the liquid are separated from one another" [25]. In mathematical terms, this constitutive equation, valid for the large class of (incompressible) Newtonian fluids is given by

$$\underline{\underline{\tau}} = \eta \underline{\underline{\dot{\gamma}}}, \tag{2.4}$$

with η being the shear viscosity (SI units of $\mathrm{Pa} \cdot \mathrm{s}$). Here $\underline{\underline{\dot{\gamma}}}$ is the rate of strain (or shear rate) tensor given by

$$\underline{\underline{\dot{\gamma}}} = \nabla \underline{v} + (\nabla \underline{v})^T. \tag{2.5}$$

Eqs. (2.2) and (2.4) together with the consideration of mass conservation and incompressibility ($\nabla \cdot \underline{v} = 0$) result in the well known incompressible Navier-Stokes equations. On the other extreme, the constitutive equation for ideal solids, is described by Hooke's law of solids

$$\underline{\underline{\tau}} = G \underline{\underline{\gamma}}, \tag{2.6}$$

where $\underline{\underline{\gamma}}$ is the strain and G is the elastic (or Young's) modulus and is a fourth order tensor in the general case. [24]

In complex fluids neither Eq. (2.4) nor Eq. (2.6) can be regarded as a successful model. However, for a quite broad class of complex fluids the steady state stress can be described by generalizing η in Eq. (2.4) to be a function of $\|\dot{\gamma}\|_{L_2}$. This is the so called generalized Newtonian fluid (GNF) model [24]. Since in the remainder of this thesis only simple shear flow will be encountered $\|\dot{\gamma}\|_{L_2}$ will be denoted by $\dot{\gamma}$ and the corresponding shear stress by σ. A schematic description of the typically observed behavior is shown in Fig. 2.1. For the case of Newtonian behavior, the dependence between the shear rate and the shear stress is linear. Another large group of fluids steady state behavior is characterized by a power-law type behavior. Here fluids for which the power law exponent is smaller than one are called shear thinning and those for which the exponent is larger than one are shear thickening. Of these two effects shear thinning is the more common one [26].

σ_c in Fig. 2.1 is called the yield stress. Loosely speaking yield stress fluids, i.e. fluids with a yield stress, behave like solids below the yield stress and flow like fluids above it. Typical flow curve models (Fig. 2.1) for yield stress fluids are the Bingham and Herschel-Bulkley ones [27]. In the Herschel-Bulkley model the stress follows the equation

$$\sigma = \sigma_c + \tilde{\eta} \dot{\gamma}^n, \tag{2.7}$$

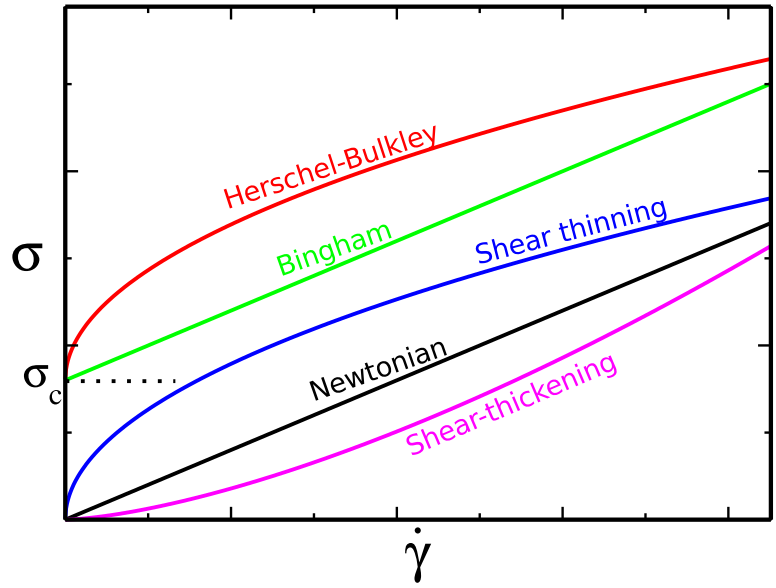

Figure 2.1. Schematic representation of typical flow curves observed in complex fluids.

were $\tilde{\eta}$ and n are material parameters. The Bingham model is recovered for $n = 1$. There exists still some controversy of the nature of the yield stress and its definition [13, 14]. By making a distinction between thixotropic and simple yield stress fluids many problems related to yield stress fluids can be resolved [28]. Hereby the former ones show time dependent behavior while for the latter ones any time dependence can be normally neglected. The emergence of a yield stress can be understood as a jamming transition. The jamming phase diagram proposed by Liu et al. [29] describes qualitatively the interplay between density, load and temperature on the jamming transition for repulsive systems. Shortly after Liu *et al.* [29], Trappe et al. [30] proposed a jamming phase diagram for slightly attractive particles. The jamming phase diagrams only address the existence of a finite yield stress, while many open questions about yield stress fluids persist [22, 23].

More often than not, merely knowing the steady state flow curve is not sufficient, instead also the transient behavior has to be addressed. Traditionally the term thixotropy has been used to describe "the continuous decrease of viscosity with time when flow is applied to a sample that has been previously at rest and the subsequent recovery of viscosity in time when the flow is discontinued", but its definition may vary depending on the source [12]. The term thixotropic yield stress fluid is now used to denote yield stress fluids with a non-monotonic flow curve [17]. But, as

recently pointed out by Fielding [31], strictly speaking practically all complex fluids show some time dependence [32]. Fielding proposes to term the yield stress fluids with non-monotonic flow curves viscocity bifurcating yield stress fluids [31]. As this discussion shows there is still the possibility for confusion regarding the terminology, and further changes are to be expected.

2.2 Complex fluids

Which fluids show complex behavior? The class of complex fluids under consideration in this thesis are those which have some internal structure [28]. In particular, these are systems of several phases such as colloidal suspensions, emulsions and foams. Further, the suspending media will be Newtonian. The topic is broad and several recent specialized reviews exist [33, 22, 34, 23]. Here only a short review on the current status of the key observations of interest is given.

The simplest case is obtained when considering density matched, non-interacting spheres (hard spheres) in a Newtonian fluid. At sufficiently low concentrations, these suspensions behave Newtonian with a viscosity that is higher than that of the suspending fluid and only a function of the concentration. Depending on whether the spheres are Brownian or not, above a certain concentration ϕ, the behavior changes. Brownian suspensions go through a glass transition as $\phi \to \phi_g$ [35], while for non-Brownian particles the viscosity diverges as $\phi \to \phi_j$, where ϕ_j is the volume fraction at random close packing [36]. Soft, deformable particles such as emulsions behave mostly similar to hard sphere systems at low concentrations. However, when soft particles are confined above ϕ_j they obtain Herschel-Bulkley like flow curves [37].

The introduction of interactions modifies the fluids behavior. Repulsive interactions at moderate concentrations and shear rates only modify the rheology slightly [37], while slight attractive interactions in hard non-Brownian particles lead to yield stress behavior below ϕ_j [38]. A system that is much less understood are those of unstable colloidal dispersions [39]. Here the particles can aggregate/flocculate and be broken up due to the presence of shear.

The rheology of particle suspensions is heavily affected by the particle shape. For rigid rod like particles at low concentrations the behavior follows the model by Jeffery [40] and at slightly higher concentration, an

effective diffusivity can account for the inter particle interactions [41]. For aggregating fiber suspensions, the rheology of the system gets more complicated and is not that well understood. The current understanding is that these can be either dominated by cluster formation through aggregation and fragmentation or be additionally affected by orientational effects [42, 43, 44].

2.2.1 Nanocellulose suspensions

Here a short review on the main characteristics of nanocellulose and their water suspensions is given. The term nanocellulose comprises a large group of fibrous materials obtained from cellulosic raw materials. The term is adequate if at least one dimension is between $1 - 100$ nm. There is a wide range of potential applications e.g in the paper and board industry [45], utilization in various composites [46, 47], as rheology modifiers [48], and in medical applications [49]. The properties of the obtained fibers depend on the raw material and the fabrication method [4].

One route to obtain nanocellulose is via acid hydrolysis of cellulose fibers. The resulting fibers have typically diameters of 2-20 nm and are relatively short compared to the original cellulose and have a broad size distribution with typical lengths between 100 to 600 nm [50, 4]. These rod-like fibers are now mostly termed nanowhiskers, but also several alternative names are in use, e.g. nanocrystalline cellulose (NCC) and cellulose nanocrystals (CNC) [51]. Stabilized, i.e. non-aggregating suspension of nanowhiskers at sufficiently low concentrations behave like rod-like particles in fluids [52, 51]. The stability is for example affected by the acid used in the hydrolysis process [51]. Nanowhiskers will however not be further addressed in this thesis. More specialized discussions on the topic can be found for example in Refs. [53, 51].

Nanocellulose can also be obtained via direct mechanical disintegration of wood or other cellulosic fibers. This was first realized in the 1980's by Tubarak [48] and Herrick [54]. The resulting fibers are termed microfibrillated cellulose (MFC) and have a broad size distribution with diameters at the hundred nanometer range [4]. Most importantly, MFC fibers are considerably longer and have a higher aspect ratio compared to nanowhiskers. The energy consumption of the mechanical disintegration process is however very high, which has lead to the development of other approaches. The combination of chemical pre- and post treatments in addition to the mechanical disintegration have proven to be a viable option

in this regard [4]. One popular method is the combination of an enzymatic hydrolysis pretreatment and mechanical disintegration [55]. The resulting MFC consists of fibers with diameter 5-6 nm and fibril aggregates with diameter 10-20 nm and length of several micrometers [55]. Another approach is to use TEMPO-mediated oxidization prior to the disintegration [56, 57]. In addition to lowering the total energy consumption, this pretreatment also introduces a negative charge on the cellulose fibrils, which increases the electrostatic repulsion between the fibers. The resulting fibers have diameters from 3-4 nm, which suggests that these are formed of individual microfibrils. Depending on the oxidation and disintegration methods the length varies and can be up to $2\ \mu\mathrm{m}$ [58]. In this thesis the nomenclature is as follows: MFC is used for the fibers obtained via direct mechanical disintegration. Fibers produced by TEMPO-mediated oxidization will be called nanofibrillated cellulose fibers (NFC) because of their smaller size compared to MFC. However, it should be pointed out that another frequently used term for NFC is TEMPO-oxidized cellulose nanofibers (TOCN) [58].

The main rheological properties of M/NFC water suspensions are discussed below. A more specific discussion will be presented in Section 3.3. Due to the high aspect ratio, M/NFC are effective rheology modifiers. For instance, yield stress like behavior can be obtained already at very low concentrations [7, 5]. Further both MFC and NFC suspensions are highly shear thinning and show time dependent flow behavior [59, 7]. Besides the raw material and the fibrillation process, the rheology of MFC and NFC suspensions is also affected by the temperature [7], pH [55, 6] and the ion concentration [60, 8, 9].

2.2.2 Cellulose fiber suspensions

Even though not further addressed in this thesis, cellulose fiber suspension are discussed below, in order to give a coherent picture. Pulp fibers have typical average length of 1-3 mm and diameter 15-30 $\mu\mathrm{m}$ and are thus considerably longer and thicker than both NFC and MFC [61]. Because of this, Brownian effects can be mostly neglected. The diluteness of pulp fiber suspensions is frequently characterized through the so called crowding factor [62]

$$N = \frac{2}{3}\phi\left(\frac{L}{d}\right)^2, \tag{2.8}$$

which is the average number of fibers inside a sphere of diameter L. Here ϕ is the volume concentration of the fiber material in the suspension and d is the diameter of the fibers. The crowding factor scales with the aspect ratio squared which demonstrates that for fiber suspension many particle interactions have to be taken into account at much lower concentrations than for more spherical particles (aspect ratio close to one). For $N \ll 1$ fiber-fiber interactions can be neglected and the fiber suspension is in the dilute regime. For $1 < N < 60$ fiber-fiber interactions have to be taken into account and the suspension is said to be in the semidilute regime. However, the suspensions behave as essentially dilute up to the so called gel crowding number $N = 16$ [63, 64]. For $N \gg 60$ the suspensions are in the concentrated region. [61]

It is important to keep in mind that pulp suspensions differ from rigid rod fiber suspensions in that the pulp fibers are flexible and the fibers in pulp suspensions are not of uniform size. Further cellulose fibers swell in water and and pulp suspensions are not purely cellulose fibers and water. Due to these reasons, pulp suspensions behave only to a limited extend similar to synthetic, hard rod suspensions. One particular issue, which differs from the hard rod behavior, is the flocculation of pulp fibers. Nevertheless, studies of hard rod like fibers can give useful information about pulp suspensions. [61]

When addressing multiphase fluids, such as pulp suspensions, from the modeling perspective, different options are available and the proper choice depends on several factors such as the size scale, the concentration range and the flow regime of interest. The fluid phase is standardly modeled at continuum level (Euler approach), however other methods such as smoothed particle hydrodynamics [65] do exist. In pulp suspensions, the Euler-Lagrange approach, where individual fibers are modeled, is due to computational restrictions, currently limited to simulations at centimeter level size scales [66]. In these particle-level simulations the fibers are frequently modeled as connected spherical (or ellipsoidal) beads. From the particle level simulations many fundamental questions such as different concentration regimes and the importance of friction between fibers in the flocculation have been addressed [67].

For modeling industrially relevant size-scales and geometries such as the headbox of a paper mill, a Lagrange-Lagrange approach, is often computationally feasible. For dilute suspensions, it suffices to model the orientation probability distribution and the local fiber concentration (see e.g.

[68]). The flocculation effects in pulp fiber flows, important above the dilute regime, have been modeled by utilizing population balance equations [69, 70]. Relatively few studies employ a two-way coupling between the flow and the fibers in the Lagrange-Lagrange approach (see e.g. Krochak *et al.* [71]) for an exception). The industrially relevant turbulent regime further increases the complexity of the models. It is known from experiments that fibers reduce velocity fluctuations. Further the fiber orientation distribution is randomized by turbulence. [66]

In the concentrated regime pulp suspensions obtain a yield stress and are standardly addressed utilizing GNF models, mostly the Herschel-Bulkley model [72]. However, it has been recently experimentally shown that sufficiently concentrated pulp suspensions exibit thixotropic properties, which would warrant structural models [73, 74].

As these discussion demonstrates, while simulation techniques deliver undoubtedly valuable information, there is still considerable room for improvement. More about the state-of-the-art modeling of pulp suspensions can be for example found in the recent reviews by Hämäläinen *et al.* [75, 66] and Derakhshandeh *et al.* [61] and the references therein.

2.3 Rheometry

In order to test the dependence between deformation and resulting stresses, one needs to perform rheometry. While the emphasis in this thesis lies in modeling, it is elementary to understand also the associated experiments and thus a short discussion on this topic is in order. Normally macroscopic displacement and forces are measured from which the stresses and deformations can (under certain assumptions) be deduced. In certain cases, it is also possible to measure the stresses directly for example through flow birefringence [76].

Specialized rheometers for different flow situations, for example shear and elongational flow, exist. A more in-depth discussion on different rheometer types can be for example found in [77], here only the most relevant ones for this thesis will be addressed. The particular class of rotational, drag flow rheometers can be deemed especially suitable for the study of complex fluids with very long relaxation times, since the applied strain is not limited. This is not the case in, for example, pipe or extrusion rheometers. The main geometries for rotational rheometers are plate-plate, cone-plate and concentric cylinder. These rheometer types are schematically

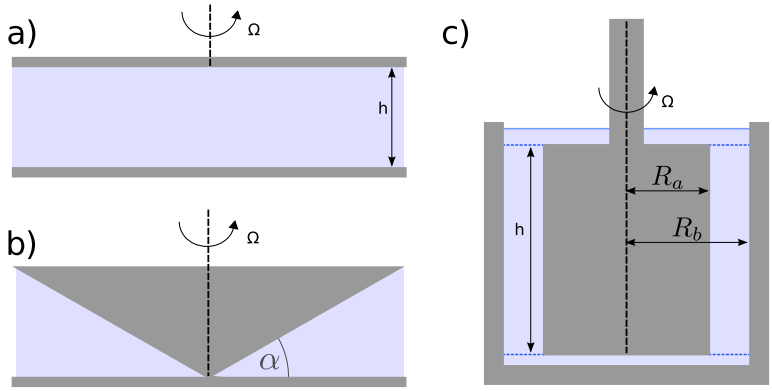

Figure 2.2. Schematic representation of different rotational rheometer geometries: a) plate-plate b) cone-plate c) Couette or concentric cylinder geometry. The view is from the side.

depicted in Fig. 2.2.

A typical task in rheometry is to measure the steady state flow curve (Fig. 2.1). Other standard measurements include shear rate or stress start-up measurements. In practice, the applied torque and the rotational velocities are measured. From these values, the shear rate and stress are extracted.

Besides measurements at steady shear rate or stress, oscillatory measurements are routinely performed. Oscillatory measurements are not within the scope of this thesis, but are here shortly discussed for completeness. In small amplitude oscillatory shear (SAOS) measurements, which are in the linear viscoselastic regime, viscoelastic and viscous contributions, termed storage and loss modululus respectively, are calculated from the measured quantities. Oscillatory measurements beyond the linear viscoelastic regime, so called large amplitude oscillatory shear (LAOS) measurements, can be analyzed through various methods [78]. Yet another approach is to apply small strain oscillatory motion during steady shearing [79, 80, 81, 82].

In traditional rheometry as discussed above, only averaged quantities are measured. Additionally, a large amount of research is now also devoted to spatially resolved measurements in combination with traditional rheometry. Different methods for accessing spatially resolved information are becoming more widespread and developed. Such techniques include ultrasonic speckle velocimetry (USV) [83], optical coherence tomography (OCT) [84], and magnetic resonance velocimetry (MRV) [85]. Spatially resolved rheometry reveals more information than what traditional rhe-

ology on its own can provide [77].

2.3.1 Complex behavior in simple shear rheometry

When dealing with complex fluids, several factors can complicate the rheometric measurements. For calculating the shear rate and stress from the measured quantities via the standard methods, certain conditions have to be fulfilled. In particular these include no-slip boundary conditions, homogeneity of the sample at the measurement scale and that a reproducible steady state is reached during the measurement. However, these criteria are not necessarily met, especially when dealing with thixotropic yield stress fluids. The spatially resolved measurements have reinforced this view and also led to the discovery of new effects, which can arise in even seemingly simple fluids and rheometrical experiments, such as in start-up flow of simple yield stress fluids [19, 20].

In complex fluids the no-slip boundary condition is not a good approximation because of a layer of relatively lower viscosity close to the wall. This results in an effectively lower shearing of the bulk material compared to the case with no slip, since the low viscosity layer will be highly sheared. This effect is termed apparent wall slip. In Ref. [21] Buscall discusses the importance of properly addressing wall slip. He states that wall slip should not be thought of as merely nuisance, but rather as a property of the fluid at hand. A similar kind of mind set is also appropriate for many other effects that can arise in complex fluids. For example flow heterogeneity in terms of the existence of different shear rates at the same stress, which is termed shear banding, is known to arise in thixotropic yield stress fluids, and is due the existence of a negative slope in the intrinsic flow curve [86, 87]. However, even in simple yield stress fluids, which were previously assumed to always flow homogeneously, longlived transient shear bands have been observed in flow start-up experiments [19, 20]. The observed transient shear banding during flow start-up of a Carbopol gel at constant shear rate of by Divoux *et al.* [19] is reproduced in Fig. 2.3. In the figure the evolution of the transient shear band is clearly seen. However, after a rather long time a homogeneous steady state is finally reached. In addition, many other issues, such as the initial state from which the experiments are started can affect the results of rheometric measurements. The phenomena introduced here will be addressed in more detail in Chapter 3 of this thesis.

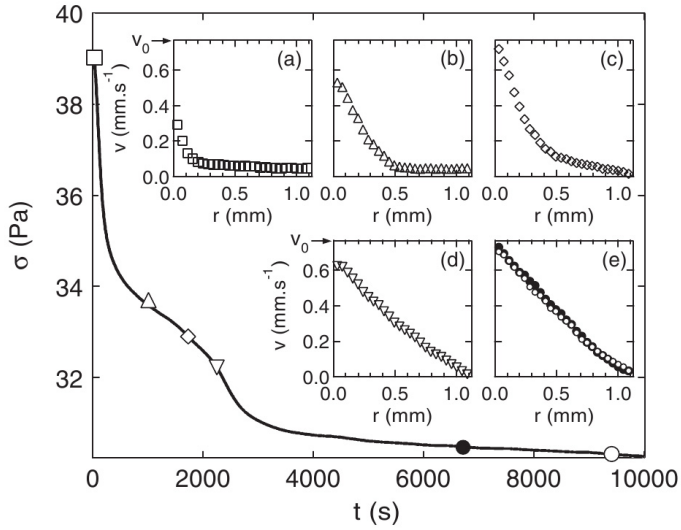

Figure 2.3. Stress evolution during shear rate controlled flow start-up observed in Carbopol by Divoux *et al.* in concentric Couette geometry. The local velocity profiles are shown for the times indicated in the stress figure. Reprinted figure with permission from Ref. [19]. Copyright (2010) by The American Physical Society.

2.3.2 Cylindrical Couette geometry

The concentric cylinder Couette geometry is of special interest in this thesis. For this geometry, the stress distribution inside the device is known. Neglecting end effects and under creeping flow conditions, the stress inside the rheometer is given by

$$\sigma(r) = \sigma_{R_a} \frac{R_a^2}{r^2}, \tag{2.9}$$

where σ_{R_a} is the stress measured at the boundary and R_a is as given in Fig. 2.2 c).

The local shear rate inside the Couette device, $\dot{\gamma}_{r\phi} = r\frac{d\omega}{dr}$, is given by (assuming viscous flow only) [88]

$$\dot{\gamma}(r) = \frac{\Omega}{r^2 \mu(r) \int_{R_a}^{R_b} \frac{1}{r^3 \mu(r)} dr}, \tag{2.10}$$

where Ω is the angular velocity (see Fig. 2.2 c)).

Often, one can reasonably assume that the viscosity is approximately constant above the gap. In this case one obtains for the shear rate at the rotor

$$\dot{\gamma}_a = \Omega \frac{2R_b^2}{R_b^2 - R_a^2}, \tag{2.11}$$

which is only a function of the device geometry and the angular velocity.

2.4 Modeling

Here the theory related to the models utilized in this thesis is presented.

2.4.1 Viscosity functions

For very dilute, mono-disperse suspensions of hard spheres in a Newtonian suspending fluid of viscosity η_s, the effective viscosity is given by the well known Einstein equation [89, 90]

$$\eta = \eta_s(1 + \frac{5}{2}\phi), \tag{2.12}$$

where η is the effective viscosity and ϕ is the volume fraction of the solid phase. For slightly more concentrated suspensions a second order term accounting for pair-wise interactions has to be included [91]. However, for concentrated suspensions, many-body interactions have to be taken into account. Many different, mostly empirical, functions for this regime exist (see for instance [92]). The viscosity function utilized in this thesis is [88]

$$\eta_r = \left(1 - \frac{\phi}{\phi_m}\right)^{-\kappa}, \tag{2.13}$$

where η_r = (η/η_s) is the relative viscosity. Eq. (2.13) states that the relative viscosity η_r diverges as ϕ approaches ϕ_m with and exponent of $-\kappa$. The Krieger-Dougherty model ($\kappa = 2.5\phi_m$) [93] and the model obtained by Maron and Pierce [94] and Quemeda [95] ($\kappa = 2$) emerge as special cases of Eq. (2.13).

2.4.2 Particle migration

The equations above can be used in the case of a homogeneous concentration profile. However, migration of particles due to shear can lead to inhomogeneous concentration profiles. The migration can be modeled via a flux term N which results in a change in the volume fraction

$$\frac{d\phi}{dt} = \nabla \cdot \mathbf{N}. \tag{2.14}$$

In Publication V the diffuse flux model proposed by Phillips et al. [88] is used, which has been shown to describe the steady-state concentration profiles satisfactorily [96]. In this model shear induced migration results from two distinct effects. The main assumptions in this model are that the frequency of particle-particle interactions (collisions) scales as $\dot{\gamma}\phi$ and that each interaction results in a displacement of the order of one particle radius a perpendicular to the stream lines.

The first effect is due to a change in interaction frequency. From the main assumptions it follows that the difference of interaction frequencies is of the order of $a\nabla(\dot{\gamma}\phi)$ across one particle diameter. Together with the assumption about the displacement at each interaction this leads to an average drift velocity which scales as $a^2\nabla(\dot{\gamma}\phi)$ and thus the flux

$$\mathbf{N_c} = -K_c a^2(\phi^2\nabla\dot{\gamma} + \phi\dot{\gamma}\nabla\phi), \tag{2.15}$$

where K_c is a rate constant of order unity. [88]

A second source for migration is a spatially varying viscosity. The drift velocity is assumed to be proportional to the relative change in viscosity $(a/\eta)\nabla\eta$. This results together with the main underlying assumptions in the flux term

$$\mathbf{N}_\eta = -K_\eta\dot{\gamma}\phi^2\frac{a^2}{\eta}\frac{d\eta}{d\phi}\nabla\phi, \tag{2.16}$$

where K_η is a rate constant of order unity. [88]

2.4.3 Aggregation and fragmentation – Population balance equations

Unstable colloidal dispersions exhibit a plethora of different phenomena [97]. The aggregation and fragmentation mechanism can be addressed on a continuum scale via population balance equations (PBE) [98, 99, 100]. Von Smoluchowski formulated the mass balance equations already in 1917 [101]. For the discretized version, which includes aggregation and fragmentation, the evolution of the number density n of species i reads

$$\frac{dn_i}{dt} = \frac{1}{2}\sum_{j=1}^{i-1} k^{(a)}(i-j,j)n_{i-j}n_j - \sum_{j=1}^{\infty} k^{(a)}(i,j)n_i n_j - k^{(b)}(i)n_i + \sum_{j=i+1}^{\infty}\beta(i,j)k^{(b)}(j)n_j, \tag{2.17}$$

where $k^{(a)}$ and $k^{(b)}$ are the aggregation and breakage kernels respectively and β is the breakage function. These terms will be discussed below. The first term on the right hand side of Eq. (2.17) accounts for a gain in number density due to aggregation of smaller classes, the second term accounts for loss due to aggregation to larger classes, the third term accounts for a loss due to fragmentation, and the last term for a gain due to fragmentation of larger classes. The $1/2$ in the first term accounts for double counting, and for the special case where i=j the term emerges from the fact that the number of pairs of two is $1/2(N(N-1)$ (for N aggregates) which is $1/2N^2$ in the thermodynamic limit [102].

PBEs are broadly utilized in various fields [103]. Hereby the physics enters via the kernels: these describe the mechanisms that cause aggregation (k^a) and fragmentation (k^b). For the case considered here, the driving mechanisms are Brownian motion and laminar shear. The Brownian aggregation kernel emerges from the fact that the rate at which particles of diffusivity D hit a sphere of radius r is $4\pi Dr$. Further, for a pair of spherical particles the substitution $r = r_i + r_j$ and $D = D_i + D_j$ can be made. Using for the diffusion the classical result $D = k_B T/(6\pi\eta r)$, leads to the perikinetic aggregation kernel

$$k_p(i,j)^{(a)} = \frac{2}{3\eta_0} k_B T (r_i + r_j)/(1/r_i + 1/r_j), \tag{2.18}$$

where k_B is Boltzman's constant. [101]

Von Smoluchowski considered also the case of aggregation due to laminar shear from the assumption that the particles follow streamlines. The rate at which a particle of size i is hit by particles of size j is given by $\frac{4}{3}\dot{\gamma} n_j (r_i + r_j)^3$. Thus it follows that the aggregation kernel for laminar shear is given by [101]

$$k_o^{(a)} = \left(\frac{4}{3} \dot{\gamma} (r_i + r_j)^3 \right). \tag{2.19}$$

The kernels in Eq. (2.18) and 2.19, overestimate the collision frequency in most practical applications. In order to account for the interaction potentials and reduced permeabilities the kernels are scaled by a collision efficiency c smaller than unity [104]. Methods for estimating the collision efficiency such as a capture cross-section method [104] and a stability ratio [99] exist. However, in Publication I a constant value for the collision efficiency is used, which is sufficient since no quantitative fitting to experimental data was done. Moreover, in order to study the combined effect of perikinetic and orthokinetic aggregation, in Publication I the superposition of the two kernels [105, 106] with two separate collision efficiencies is used

$$k^{(a)}(i,j) = c_p k_p^{(a)}(i,j) + c_o k_o^{(a)}(i,j). \tag{2.20}$$

In particular, c_o is assigned a constant value whereas c_p is varied to study the influence of Brownian (perikinetic) aggregation.

For the fragmentation process different formulations exist in the literature [107, 108]. The fragmentation kernel utilized in Publication I reads

$$k^{(b)}(i) = \dot{\gamma} \ \exp\left(-\frac{2F_c}{5\pi\rho_i^2 \eta \dot{\gamma}} \right), \tag{2.21}$$

where F_c is a parameter modeling the aggregate effective bond force. The fragmentation rate grows rapidly if the hydrodynamic force grows

larger than F_c. This kernel has been shown to reproduce experimental results [43]. In order to model the fragmentation process, also information on how an aggregate breaks up is needed. Different processes such as erosion and splitting are implemented via the breakage function $\beta(i, j)$. In Publication I binary fragmentation was used.

Through the methods discussed above, the evolution of the aggregate number densities can be modeled. In order to couple the aggregate state to the flow, the aggregate radius is modeled via fractal scaling

$$r_i = r_0 \left(\frac{i}{C} \right)^{1/d_f}, \tag{2.22}$$

here r_0 is the size of the primary particle in the aggregate i, and d_f is the fractal dimension. C is the packing density of the particles and it is generally assumed to be of order unity. [100] From the aggregate radius the effective jammed volume fraction can be obtained straightforwardly

$$\phi = \frac{4}{3}\pi \sum_i n_i r_i^3. \tag{2.23}$$

The viscosity is then obtained through Eq. (2.13).

2.4.4 Structural models

As it is clear from the discussion in Section 2.2, there are different origins for the non-linear behavior of complex fluids. The PBE model which was explained above, models the specific case of structure evolution due to aggregation and fragmentation. However, often one is interested in modeling the rheological behavior at phenomenological level and in general trends shared between different kinds of fluids. Typically, structural models are used in this case. Then, a scalar parameter (often λ) is utilized as a structure parameter, modeling the degree of jamming. Structural models are also the preferred choice, when one does not have information on parameters needed in more complex models. Additionally, computational limits pose restrictions on feasible models. One of the simplest and best known λ-models that has proven very useful for addressing the differences between simple and thixotropic yield stress fluids is that proposed by Coussot et al. [16]. There the evolution of structure reads

$$\frac{d\lambda}{dt} = \frac{1}{\tau} - \alpha\lambda\dot{\gamma}. \tag{2.24}$$

Here the first term on the right hand side models aging and the second term shear rejuvenation. There exists a plethora of different structural

models, however most of them feature the same mechanisms: structure buildup due to shear or Brownian motion and reduction in structure due to shear. A more detailed discussion on structural models can be found in Refs. [109, 12, 23].

In this thesis two different structural models will be used. Both are written in the terminology of changes in the jammed volume fraction ϕ as in the PBE model. Similarly, the viscosity is a function of ϕ and is given by Eq. (2.13). In the first model, utilized in Publication II, the evolution of ϕ is given by

$$\frac{d\phi}{dt} = \frac{A_b}{(\eta/\eta_o)^m} + (A_s - B_s\phi)\left(\frac{\dot{\gamma}}{\dot{\gamma}_0}\right)^k, \tag{2.25}$$

here the first term on the right hand side models shear independent (A_b, η_0, m) growth, while the second term models both shear dependent growth and breakage (A_s, B_s, and k) of ϕ. k adjusts the volume fraction sensitivity to shearing. This model was previously studied by Illa *et al.* [110] and it was found to capture qualitatively features of the fluidization of a simple yield stress fluid. The model can be tuned to have a Herschel-Bulkley (Eq. (2.7)) like flow curve, however, the exponent is fixed to one.

A slightly different model was formulated in Publication IV in order to model flow curves with Herschel-Bulkley exponents different from one. In this model the volume fraction $\phi \in [0, 1]$ (i.e. $\phi_{max} = 1$). The time evolution reads

$$\frac{d\phi}{dt} = A(1-\phi) - B\phi, \tag{2.26}$$

where A is the rate of structure growth and B that of structure decomposition. Again shear independent growth and shear dependent growth and breakage are implemented in the following form

$$A = \alpha\tau + \beta\tau\dot{\gamma}^k \tag{2.27a}$$

$$B = \tau\dot{\gamma}, \tag{2.27b}$$

here α, β, τ and k are fitting parameters. The steady state is fixed by α, β, and k, while τ scales the time-evolution. Setting κ in Eq. (2.13) to unity enables a simple analytical solution for the steady state flow curve with a Herschel-Bulkley like shape (with the addition of a Newtonian regime at high shear rates)

$$\sigma = \eta_0\alpha + \eta_0\beta\dot{\gamma}^k + \eta_0\dot{\gamma}. \tag{2.28}$$

With $\kappa > 1$ in Eq. (2.13) the steady state flow curve shows a negative slope i.e. that of a thixotropic yield stress fluid.

2.4.5 Other models

Many different modeling approaches for studying yield stress materials exist, and different theories might be useful to answer different things. This was emphasized by Bonn et al. in their recent review on yield stress fluids [23], and this view can be clearly extended beyond yield stress fluids to rheology modeling in general. Here a short discussion of common models, in particular the Soft Glassy Rheology (SGR) [111], and the Shear Transformation Zone (STZ) [112], is presented. Yet a different approach is to directly utilize molecular dynamics MD simulations (e.g. in [38, 113]). A more detailed review of different models can be found in Refs. [34, 23].

In the SGR model the fluid is modeled through mesoscopic elements (e.g. clusters of emulsion droplets) which undergo activated hopping events. The behavior of the SGR model is tuned via an effective temperature affecting the hopping probabilities. The hopping of an element can be understood as a local yielding event. The qualitative starting point of the SGR model thus differs from the models utilized in this thesis, which describe the behavior starting from the flowing state. In its standard form, when the effective temperature is given a constant value, the SGR model can describe simple yield stress fluids. In this form, the SGR model was shown to predict transient shear banding behavior [114, 115]. By modifying the model and connecting the effective temperature to the jump events, the flow curve can be given a non-monotonic slope i.e. that of a thixotropic yield stress fluid. This resulting model predicts steady state shear banding and viscosity bifurcation [31]. However, in the SGR model the connection between model parameters such as the effective temperature and physical fluid parameters is not clear.

The STZ model bases on the observation that in amorphous solid systems the shear deformation localizes to so called shear transformation zones. The model describes the birth and annihilation of the shear transformation zones at continuum. Thus the starting point of the STZ description is for flows starting from the the solid-like state. Recently the transient shear banding phenomena was addressed with the STZ model [116].

3. Results and discussion

This chapter discusses the main results of Publication I-V. In particular, the first part discusses Publication I which studies the simple shear rheology in aggregating colloidal systems, such as the influence of the initial state, transient and steady state shear banding. From the start-up and steady state results the focus is next turned to a more complex measurement protocol, namely shear rate sweep experiments, which are frequently utilized to measure steady state flow curves. In Publication II a structural model is employed to gain insight in the hysteresis observed during measurements. Next the lessons learned in the observations made in Publication I, II are applied to measure and model the rheology of MFC and NFC. In the last part, wall slip, which is known to play a crucial role in the flow of complex fluids, will be addressed – the topic of Publication V.

3.1 Population balance equations model

This section relates to Publication I. The research focus was in obtaining a better understanding of how the rheological behavior results from the underlying microstucture in aggregating colloidal suspensions. While structural models are able to explain many aspects of yield stress fluids [16, 110, 117], and share some qualitative aspects with the PBE model, the purpose here was to test a model with a physical interpretation for the structure parameter. Further, the aim was to test whether this more complex model would reveal new phenomena that have not been observed in the simpler models.

3.1.1 Steady state flow curves

As a starting point, model parameters obtained from a fit to latex suspensions were used [43, 118]. The resulting steady state flow-curves have Herschel-Bulkley like shape. These results were obtained without the inclusion of the perikinetic aggregation mechanisms ($c_p = 0$ in Eq. (2.20)). By including the perikinetic aggregation term via giving c_p non-zero values, the steady state flow curve is found to obtain a non-monotonic shape. Flow curves at different concentrations and with different amount of perikinetic aggregation are shown in Fig. 3.1. The appearance of the non-monotonic shape is due to the fact that while both, the aggregation due to laminar shear and the fragmentation, scale with the shear rate, the perikinetic term is shear rate independent and will thus dominate at sufficiently low shear rates. The perikinetic aggregation is an example of what the constant buildup in λ-models (e.g. [87]) could describe. The shear rate at which the derivative of the flow curve changes sign is known as the critical shear rate $\dot{\gamma}_c$. The effect of the concentration on the flow curves is also clearly seen in Fig. 3.1. It should be noted that in the figure only the concentration, (and c_p) is varied while all other parameters are kept fixed. For the case without perikinetic aggregation it is found that there is a critical concentration below which there is no yield stress. For the case with perikinetic aggregation, the existence of a yield stress emerges at lower concentrations, further, $\dot{\gamma}_c$ increases with the concentration. An increase of the $\dot{\gamma}_c$ has also been observed in experiments [87].

In the current model the inclusion of the perikinetic aggregation term leads to a situation where the stress tends towards infinity when approaching zero shear rate. The way this issue is approached here is through the consideration that at sufficiently high viscosities, perikinetic aggregation does not evolve the aggregate size distribution any further. At rest the material would thus evolve due to perikinetic aggregation until a sufficiently jammed state is reached. To simulate that, a cutoff has been applied to the Brownian aggregation kernel at sufficiently high volume fractions (viscosities). Different cutoffs were tested,with the conclusion that the actual form of the cutoff does not alter the qualitative findings. The interpretation of the low shear rate branch is that it would appear as practically jammed, or not flowing, in experimental setups. To be precise, however, in the model here, the system is always in a flowing state

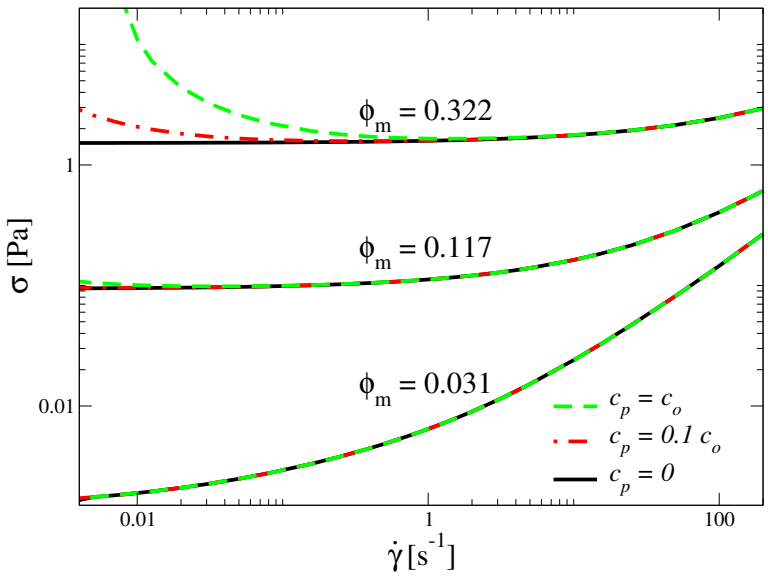

Figure 3.1. Simulated steady state flow curves for the homogeneous PBE model at different concentrations and varying amount of perikinetic aggregation. Publication I

since the stress is purely of viscous origin. Further, applying very low shear rates leads to a more jammed configuration than would be achievable through perikinetic aggregation alone.

3.1.2 Spatial behavior

In addition to the intrinsic behavior, the spatial behavior in concentric cylinder geometry was investigated in order to enable comparison with experimental findings. Here the focus was turned to the highest concentration ($\phi_m = 0.322$) as this leads to the largest spatial effects. Shear localization and shear banding inside the modeled geometry were observed. This is demonstrated in Fig. 3.2, where the simulated steady state velocity profiles at $\dot{\gamma}_a = 1\ \mathrm{s}^{-1}$ are shown. Shear localization at $c_p = 0$ is due to the stress distribution inside the Couette gap and emerges purely from the existence of a yield stress. On the other hand, shear banding is only observed in the fluids with non-monotonic flow curves. For the case with perikinetic aggregation, that showed a negative slope, the steady state results were not necessarily unique. It was found that the initial state and the driving mode can affect the steady state. The non-uniqueness is related to the position of the shear band.

These results can be best understood via the local shear rate and stress values. Examples of these are shown in Fig. 3.3 for the shear rate con-

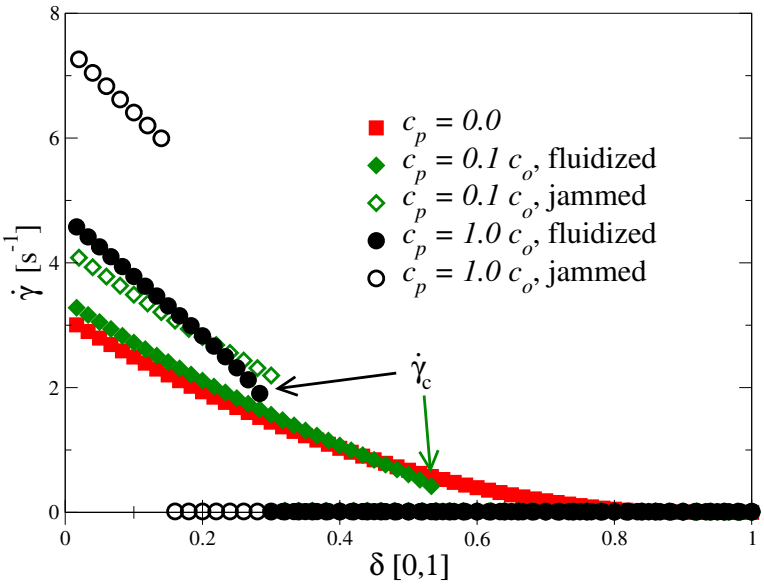

Figure 3.2. The radial distribution of shear rates in Couette gap at steady state with $\gamma_a = 1$ s^{-1} and different amount of perikinetic aggregation. Perikinetic aggregation induces a turning point to the flow curve causing the emergence of steady state shear bands in the Couette gap with critical shear rate ($\dot{\gamma}_c$) associated in between the two shear bands. Publication I

trolled case and in Fig. 3.4 for the stress controlled case together with the intrinsic steady state flow curve. The first observation is that no points lie on the unstable branch, where the stress decreases with increasing shear rate, in accordance with theory and other models [86]. For both driving modes, starting from an initially fluidized state (Fig. 3.3 a) and Fig. 3.4 a)) results in a well defined steady state, whereby the lowest flowing shear rate is $\dot{\gamma}_c$. However, when the initial state is a jammed one, the driving mode matters. In the shear rate controlled case the steady state reached by the system is determined by the dynamics of the structure evolution and the initial state and is thus not well defined. For the stress controlled mode (creep experiments) started in the jammed state, the low shear rate branch is favored. Thus in the model two well defined yield stresses can be identified for the thixotropic fluids: One obtained from the steady state flow curve (dynamic yield stress) and another, higher value (static yield stress) obtained from creep start-up experiments started from a very jammed state. At sufficiently high shear rates the steady state was found to be unique regardless of the initial state and the driving mode.

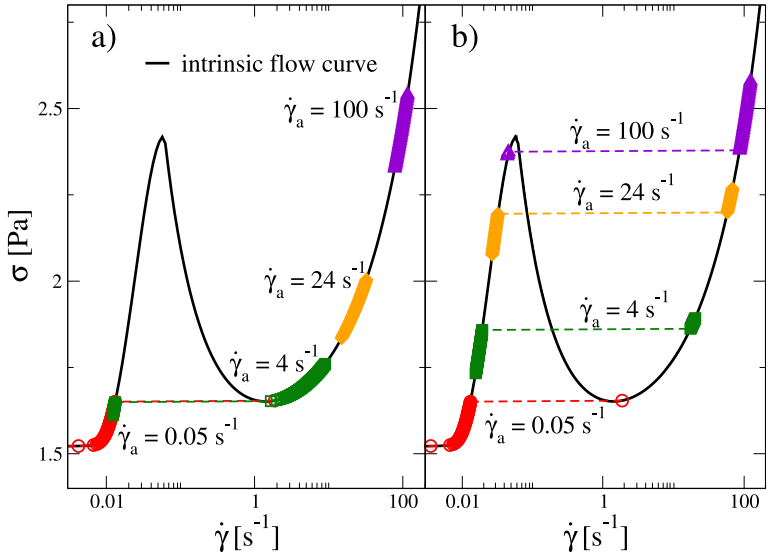

Figure 3.3. Local stress-shear rate values at steady state with the superimposed aggregation kernel at different applied engineering shear rates. When initial state is a) fluidized $\dot{\gamma}_0 = 100\ \mathrm{s}^{-1}$ b) jammed $\dot{\gamma}_0 = 10^{-5}\ \mathrm{s}^{-1}$. Publication I

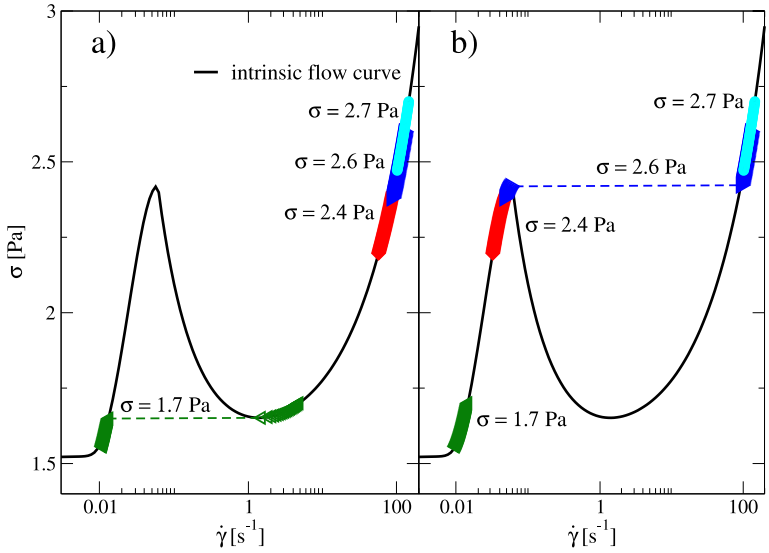

Figure 3.4. Local stress-shear rate values at steady state with the superimposed aggregation kernel at different applied stresses. When initial state is a) fluidized $\dot{\gamma}_0 = 100\ \mathrm{s}^{-1}$ b) jammed $\dot{\gamma}_0 = 10^{-5}\ \mathrm{s}^{-1}$. Publication I

3.1.3 Startup transients and fluidization times

In addition to the steady state results, the transient results are of great interest. In particular, here the focus was in the start-up evolution of the flow profile. Transients and the associated change in the aggregate size distribution for intermediate shear rate steps for the homogeneous case have been studied earlier [43] and were thus not addressed here. After a shear rate step the aggregate size distribution, and thus the viscosity, takes some time to reach the steady state value of the new shear rate resulting in stress overshoots when the shear rate is increased and undershoots when the shear rate is decreased, respectively [43]. This is typical behavior for a time-dependent fluid [12].

From the discussion of the steady state results above, several different cases of interest arise. These are in particular the transients when the initial state is the fluidized one, and when the initial state is the jammed one. When starting from the fluidized state, which resulted in well defined steady state results, it was found that the flow remained homogeneous (i.e. almost linear local velocity profile) during the evolution towards the steady state. However, at low applied shear rates, the evolution toward the steady state, namely a velocity profile with clear shear localization, and the resulting rise in stress, was found to take very long.

When starting from an initially jammed state, the results are very different. In particular even for the simple yield stress fluid, heterogeneous flow profiles, transient shear bands, were found during the start-up. Moreover, transient shear banding was observed in both, the shear rate and stress controlled case. An example of the obtained behavior is given in Fig. 3.5, which shows the stress evolution and the corresponding velocity profiles at different times during the transient for a shear rate controlled case ($\dot{\gamma}_a = 24\ \mathrm{s}^{-1}$) and with the perikinetic aggregation included. The results for the case with and without perikinetic aggregation differ in that for the thixotropic case the steady state can be shear banded, while in the simple yield stress fluid the final state is always homogeneous. These results resemble those of transient shear banding observed in Carbopol gel, with the difference that the initial elastic bulk response, and wall slip are missing from the model [19, 20].

The time it takes to reach a homogeneous flow profile is defined as the fluidization time [19]. In the model the fluidzation time was found to follow power-law scaling as a function of applied shear rate and reduced

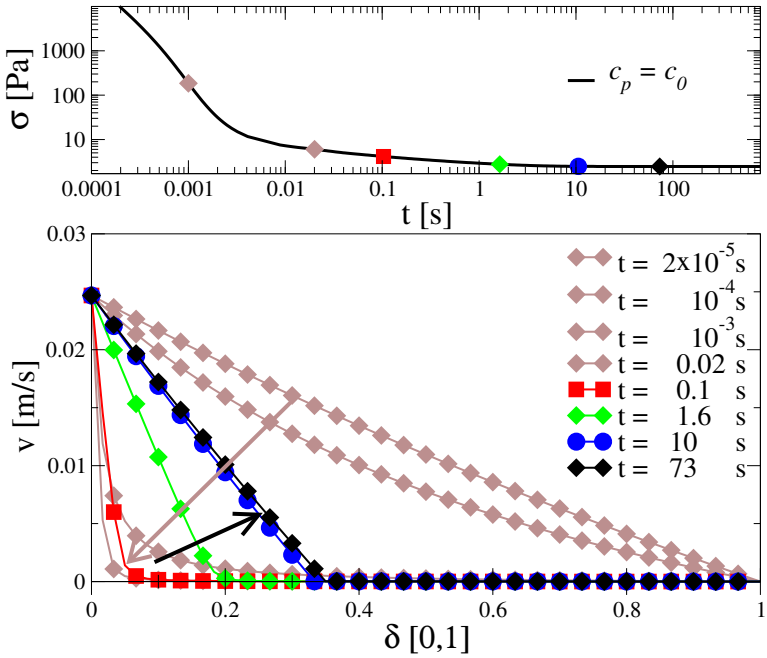

Figure 3.5. Fluidization from initially jammed state at constant applied shear rate $\dot{\gamma}_a = 24.0\ \mathrm{s}^{-1}$ for the case applying the superimposed kernel. Upper figure: Stress as a function of time. Lower figure: Velocity profiles inside the Couette gap at different times. The symbols in the upper figure are associated to the velocity profiles in the lower one. First the velocity localizes at the rotor (0-0.02 s), indicated by the upper arrow, after which the high shear rate band starts to expand (0.02-10 s) indicated by the lower arrow. The expansion of the high shear rate band slows down and finally a steady state with a shear band is reached (10-73 s). Publication I

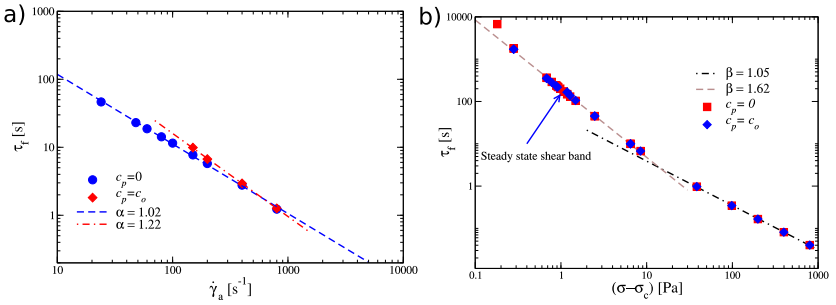

Figure 3.6. a) Fluidization times for shear rate controlled runs with superimposed and orthokinetic aggregation kernels. The dashed lines correspond to power-law fits $\tau_f \sim \dot{\gamma}_a^{-\alpha}$ at high shear rate region. b) Fluidization times for stress controlled runs with orthokinetic and superimposed aggregation kernels. $\sigma_c = 1.519$ Pa has been used. The dashed lines correspond to power-law fits $\tau_f \sim \dot{\gamma}_a^{-\beta}$. Publication I

stress ($\sigma - \sigma_y$), in the shear rate and stress controlled cases respectively (Fig. 3.6). These findings are qualitatively in line with the experimental results [19, 20] and other models [110, 117, 115].

3.1.4 Relation between aggregate size distribution and rheology

In the PBE model the aggregate size distribution is coupled to the suspension viscosity via the effective volume fraction. When all aggregates are broken down, the viscosity is at its lowest. Larger aggregates result in a larger jammed volume fraction and thus in a higher viscosity. Thus the results in the rheology measurements can be traced back to the size distribution and time evolution of the aggregates. This is not possible with structural λ-type models.

This is demonstrated in Fig. 3.7, where the aggregate size distribution is shown at different times starting from an initially jammed configuration (Fig. 3.7 a) at an applied shear rate of $\dot{\gamma} = 24\ \mathrm{s}^{-1}$. The corresponding evolution of the velocity profile is shown in Fig. 3.5. At first aggregates close to the rotor are broken down (t=0.02 s) leading to a low jammed volume fraction and thus a high shear rate close to the rotor. From the velocity profiles this could be (miss)interpreted as apparent wall slip. The aggregate size distribution takes then two different states: one expanding band, with on average smaller aggregates (fluidized band), and another which is essentially the initially jammed configuration spanning the rest of the gap. This is observed as transient shear band in the resulting velocity profile. In this case (with the perikinetic aggregation) the final state, shown in Fig. 3.7 d), is a shear banded state.

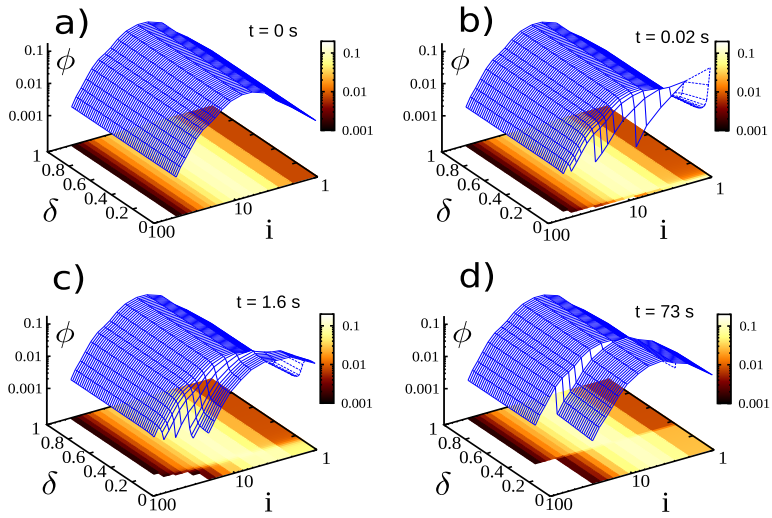

Figure 3.7. The aggregate size distribution (**i** is the number of monomers in an aggregate) at different times during flow start-up at an applied shear rate of $\dot{\gamma}_a = 24\ \mathrm{s}^{-1}$ (see Fig. 3.5) for the superimposed aggregation kernel case. a) Initial jammed configuration b) distribution broken down close to the rotor c) transient shear band has evolved d) reached steady state with (trapped) shear band. Publication I

3.1.5 Discussion

The studied model reproduces many of the features familiar from experiments for simple and thixotropic yield stress fluids and in the model it is possible to interprete these results in terms of changes in the mircrosturcture. Furthermore, the obtained results are in line with previous modeling work, reinforcing the possibility for a general approach towards the qualitative rheological behavior of soft glassy materials [115, 110, 117, 31, 23]. However, the model is qualitative and requires further comparison to other simulations and experimental work. This is since, most importantly, the kernels are derived for the dilute limit and do not take into account multiple particle collisions nor collective motion. Improving the kernels in this regard, would also make the use of the ad-hoc cutoff for the perikinetic aggregation term obsolete. Also the use of a viscosity function to model the influence of the aggregate state is an approximate scheme especially at high viscosities. Nevertheless, the qualitative model behavior, is assumed to be unaffected by these issues.

A relevant question in rheometric experiments is the influence of the initial state. In complex fluids which have an internal structure that develops at zero shear, it is important to ensure a well defined initial state for performing rheological measurements. A typical method for obtaining

the steady state is to apply a pre-shear at a high, fixed shear rate following a waiting time of fixed duration. While it can be reasonably assumed that the steady state is reached after the pre-shear, for thixotropic fluids the waiting time following thereafter results in a size distribution which is not that well defined, since during this period, the system develops via perikinetic aggregation away from the fluidized, steady state configuration. Thus the size distribution can only be obtained by the exactly same procedure. Based on the model, an initial state obtained via pre-shear without waiting time would be the preferable method for obtaining a well defined initial state, since it is possible to reach this state via many different paths.

Another relevant question is the connection between inter-particle forces and the resulting rheological behavior [23]. In Ref. [119] Ragouilliaux *et al.* tuned the rheology of emulsions by the addition of colloids. By changing the amount of colloids a transition from simple to thixotropic fluid behavior could be demonstrated. Qualitatively in line with the results obtained in Publication I, they observed for the thixotropic case shear banded flow profiles at low shear rates and homogeneous flow profiles at high shear rates which matched those of the simple yield stress fluid. In the PBE model inter-particle forces are indirectly accounted for in the collision efficiency and in the fragmentation kernel via the aggregate cohesive force. Thus increasing the attraction has two effects: an increased rate of aggregation and a higher resistance of aggregate fragmentation due to shear. In Publication I the transition from simple to thixotropic yield stress fluid was studied by changing the amount of perikinetic aggregation. This could be experimentally addressed by studying systems with different particle sizes (of the monomers). Further studies in the direction of coupling simulations and experimental data in this regard would be very interesting.

A coupling between transient behavior and the steady state has been proposed based on experimental results [20]. There it was proposed that the Herschel-Bulkley exponent (n in Eq. (2.7)) is given by the ratio of the exponent obtained for the scaling of the shear rate controlled fluidization times and that of the stress controlled fluidization times (see Fig. 3.6) [20, 23]. In its current form, the PBE model can not be utilized for addressing this coupling. This is due to the fact that the flow curve can be changed via the viscosity function (Eq. (2.13)) independent of the scaling of the fluidization times.

There are several aspects in which the PBE model could be extended. For example elastic effects are currently not accounted for since in the model the stress is purely viscous. Also wall slip and possible particle diffusion are not included. However, the extensions of the model in this regard should be coupled to experimental data.

3.2 Hysteresis

Typically flow curve measurements consist of a series of subsequent shear rate or stress steps. Frequently these ramps are performed in both directions: starting from a high shear rate or stress and step-wisely first decreasing and then increasing back up or vice versa. A difference in the resulting up and down flow curves (hysteresis) is normally taken as as a sign of time dependence of the fluid (thixotropy in its traditional sense) [12]. In Publication II a simple structural model is employed (Eq. (2.25)) to study shear rate sweeps and the associated hysteresis of simple yield stress fluids (i.e. monotonic intrinsic flow curve). The employed model shares the main characteristics with the PBE-model, such as a Herschel-Bulkley type flow curve, qualitatively similar evolution mechanisms for the structure, and emergence of transient shear banding [110]. Since the interpretation of the structure parameter in the model is not tied to a specific mechanism, the approach is quite generic.

3.2.1 Homogenous shear

Shear rate sweeps at different fixed waiting times were performed in homogeneous shear starting from an initially fluidized state – the steady state at a high shear rate. After a shear rate step, the structure evolves towards the corresponding steady state configuration. If the new shear rate is applied for long enough, i.e. the waiting time is sufficient, the steady state is reached, and one is able to infer the corresponding stress for this shear rate. However, when the waiting time is not long enough, the recorded stress merely corresponds to a transient value. In this case the deviation between the steady state results and the measured values is cumulatively increased at successive steps until the steady state is reached again at some point during the up sweep. This is demonstrated in Fig. 3.8, where the measured viscosity evolution with different waiting times is shown together with the steady state viscosity. This result is

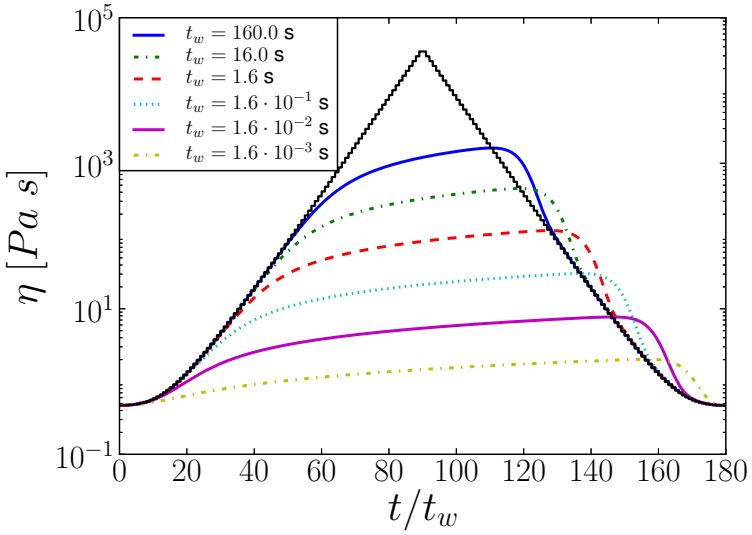

Figure 3.8. The time evolution of the fluid viscosity, η during the hysteresis cycle at different waiting times t_w. The black line represents the steady state. At smaller waiting times, the viscosity falls from the steady state line sooner. The hysteresis is a result of the asymmetry between the relaxation pattern with decreasing and increasing shear rates i.e. around the center-line here located at $t/t_w = 90$. Publication II

recovered for all systems in which the viscosity evolves qualitatively in a similar manner such as for example in the model studied in Publication I.

3.2.2 Spatial effects

In addition to the structural hysteresis discussed above, also spatial flow heterogeneities can affect the measured hysteresis. This was recently experimentally addressed for a wider range of complex fluids by Divoux *et al.* [32], where they combined shear-rate ramp measurements with time-resolved velocimetry in a Couette rheometer. In particular a hysteresis area was calculated from the shear rate and stress rate

$$A_\sigma = \int_{\dot{\gamma}_{min}}^{\dot{\gamma}_{max}} |\Delta\sigma| d(\log\dot{\gamma}), \tag{3.1}$$

where $\Delta\sigma$ is the stress difference between the up and down measurements. Additionally another hysteresis area was calculated directly from the difference in the up and down velocity profiles

$$A_v = \int_{\dot{\gamma}_{min}}^{\dot{\gamma}_{max}} \int_{R_a}^{R_b} |\Delta v| dr\ d(\log\dot{\gamma}), \tag{3.2}$$

where Δv is the spatially resolved velocity difference between the up and down measurements. Both A_σ and A_v were found to have bell like shape

as a function of waiting time. Moreover a possible coupling between the two hysteresis was suggested, since the maxima were found to appear at the same waiting time.

In order to test the generality of the proposed coupling, spatially resolved simulations were done in Publication II in addition to the ones with homogeneous shear. Here the spatial dimension was included in a similar manner as in Publication I. In these simulations slight transient shear banding could be observed during the up-sweep which resulted in additional hysteresis compared to the homogeneous model. In accordance with the experiments, the computed A_σ and A_v had both bell like shape. However, for arbitrary model parameters, the two types of hysteresis were not coupled.

3.2.3 Discussion

Based on the homogeneous shear rate sweeps it follows that in systems where the structure evolution is a function of the shear rate, a waiting time which scales inversely with the shear rate leads to better results than a shear rate independent one.

If for a certain material a coupling between the two types of hysteresis is observed, it follows that the time evolution of the underlying fluid has to be of a certain type. More experimental work where the relation of A_σ and A_v for different soft glassy materials is probed would be relevant to address the universality of the coupling. In the model, the spatial heterogeneity in terms of transient shear banding, was observed to occur during the increasing shear rate ramp. Moreover, the difference between the homogeneous and spatially resolved results is relatively small, but the importance of spatial effects was found to increase for larger gap sizes. Further it should be noticed that in Publication II only simple yield stress fluids were addressed. For the case of thixotropic yield stress fluids, it is to be expected that spatial effects play a greater role.

Similarly to Publication I wall slip was not implemented in the model utilized in Publication II. Nevertheless, wall slip was observed experimentally [32] and it could play a significant role in the observed behavior. Better understanding of the boundary conditions for different kinds of yield stress materials is clearly needed.

3.3 Rheology of nanocellulose

Measuring the rheology of nanofibrillated cellulose suspensions has turned out to be difficult. Most importantly, wall slip constitutes a serious problem in the measurement [120]. Due to the highly non-linear flow curves, shear banding, shear localization and rheological hysteresis have to be considered when interpreting and performing rheometric measurements [19, 20, 17, 32, 121]. This section discusses Publication III and IV in which exactly these issues were addressed.

3.3.1 Wide gap vane geometry

For addressing the observed slip [120], the (wide gap) vane type geometry has proven to be the method of choice in several cases where the suspension is shear thinning and prone to wall slip [122, 61]. Further, it has been proposed to use the low shear rate viscosity value measured in this geometry for the characterization of nanocellulose [123]. Numerical simulations have shown that the use of the vane geometry is equivalent to the concentric cylinder geometry for sufficiently shear thinning fluids [124]. A wide gap also efficiently diminishes possible issues that could be due to too small measurement geometries [125, 121]. However, the use of such a wide gap has as a consequence that even in the ideal case, where the flow is homogeneous above the whole gap, the stress heterogeneity has to be accounted for i.e. it is not possible to calculate the shear rate using the standard narrow gap approximation (Eq. (2.11)). This follows from the fact that for complex fluids the viscosity is a function of the stress (see Fig. 2.1), and can not be considered to be constant above the whole gap, as it is done in Eq. (2.11). In the concentric cylinder geometry, this is known as the Couette inverse problem. When dealing with yield stress fluids one option is to use a summation method [77, 126].

$$\dot{\gamma}(M) = \sum_{p=0}^{\infty} \left[2M \left(\frac{R_a^2}{R_b^2} \right)^p \frac{\delta \Omega}{\delta M} \left(M \left(\frac{R_a^2}{R_b^2} \right)^p \right) \right], \tag{3.3}$$

where M is the torque, Ω the angular velocity R_b the outer radius and R_a the inner radius. This method was utilized in Publication III. In Publication IV an alternative, iterative numerical correction scheme was used, which works also for fluids without yield stress. For flow curves which had a yield stress, the two methods were found to give similar results.

The conclusion from Publication I is that starting from an initially fully fluidized state should lead to unique results, while using an initially

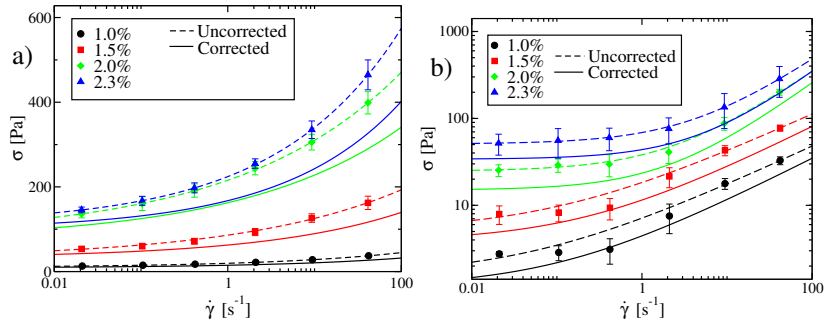

Figure 3.9. Comparison between the corrected and uncorrected flow curves of a) NFC and b) MFC. The points denote the shear rate stress values obtained with a narrow gap approximation and the dotted lines the Herschel-Bulkley fits to these. The solid lines denote the Herschel-Bulkley fits to the shear rates obtained with Eq. (3.3). Publication III

jammed state could lead to problems. These considerations were taken into account in the flow curve measurements of NFC and MFC suspensions with a bucket vane in cup viscometer (Brookfield) in Publication III. There some hysteresis was observed and the average value was used as estimate for the steady state. The importance of taking properly into account the stress heterogeneity across the gap is demonstrated in Fig. 3.9.

3.3.2 Beyond the steady state

The correction schemes, such as Eq. (3.3), for taking into account the wide gap geometry, are only strictly valid when one is dealing with the steady state in the absence of heterogeneous flows. In order to address the rheology beyond the steady state, flow curve measurements with extremely long measurement times and modeling were combined in Publication IV. In particular, the experiments were performed in a large gap vane in baffled cup geometry with NFC suspensions at concentrations in the range $0.25 - 1.0$ % (w/w), as for these the observed rheological response was that typical for a thixotropic [12] fluid. The reproducibility of the experiments was good.

In addition to flow curve measurements, stress start-up experiments were performed for the suspension at 0.5 % (w/w). The results of this measurement are shown in Fig. 3.10. The yield stress extracted from these was significantly higher than the smallest stress obtained in the flow curve suggesting the existence of a negative slope in the flow curve [16]. The initial state for performing the creep experiments was obtained by applying a constant stress below the yield stress for a fixed period prior to

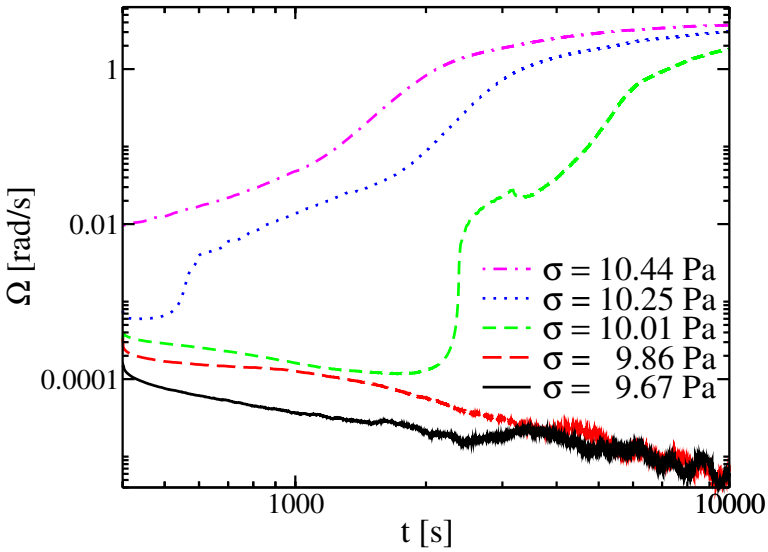

Figure 3.10. Experimental evolution of the angular vane velocity of stress controlled start-up runs for a 0.5 % NFC suspension in large gap vane in baffled cup geometry. For stresses of 10.01 Pa and above, the velocity evolves towards a finite value, while for stresses of 9.86 Pa and below the velocity continuously decreases. Publication IV

the measurements. This method was found to give reproducible results. This result is compatible with what is obtained in Publication I for stress driven runs starting from a jammed state (Fig. 3.4 b)).

The experimental shear rate sweep protocol was simulated with the model. For this, the model was first fitted against the steady state flow curve (obtained with the correction scheme for the wide gap), after which the result was improved by fitting directly against the experimental stress vs. time profile for a given protocol until a satisfactory result was achieved. Moreover, based on the experimental results, the flow curve in the model was given a negative slope and a similar cutoff as in Publication I was utilized for the constant aggregation term. Both homogeneous and spatial simulations were performed. The spatial resolution was implemented in a similar manner as in Publication I and II.

For a fixed set of parameters the time evolution of the homogeneous and the spatially resolved model in the large gap geometry were found to differ from each other. These deviations were found to be a result of the spatial evolution of the flow profile. The reason for the more pronounced spatial contribution to the rheological response compared to that in Publication II is twofold: in the measurement geometry the gap is significantly larger and additionally in this case the flow curve has a negative slope.

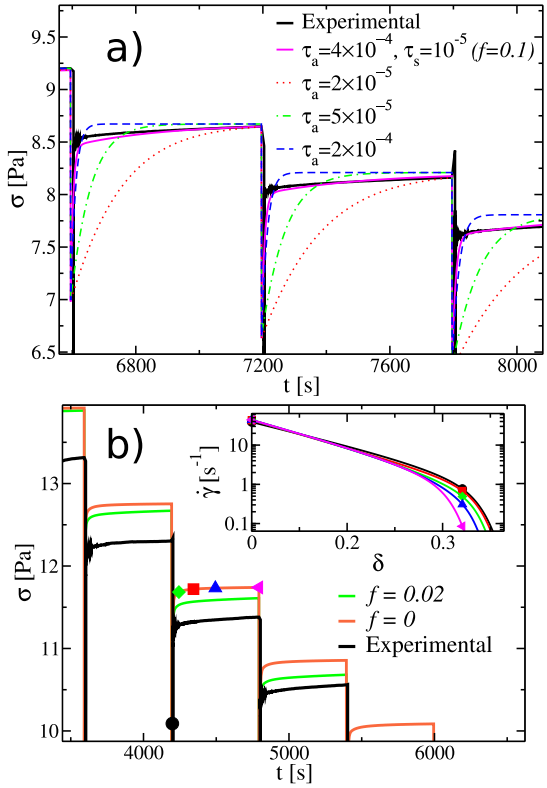

Figure 3.11. Part of the time evolution of the shear stress during the down sweep for the a) homogeneous model b) spatially resolved model. Experimental (black line) and simulated results are shown. The inset in b) shows the shear rate profile inside the gap at the times denoted by symbols in the larger figure. Publication IV

During the down-sweep the spatial contribution was via a slowly evolving shear localization, while during the up-sweep (transient) shear banding was found. Moreover, the time evolution of the spatially resolved model was closer to the experimental results which suggests that similar spatial effects as the ones occurring in the simulation might be at play in the experiments. An example is shown in Fig. 3.11 which shows the simulated time-evolution of the homogeneous and the spatially resolved model.

Another relevant observation can be made for the stress evolution after the first increasing shear rate step. In the experiments, immediately after the increase in the shear rate, the stress first overshoots after which it starts to decrease, in accordance with normal thixotropic behavior. However, thereafter the stress starts to slowly rise again. This behavior is not compatible with the structural model, nor for example with standard viscoelastic response [12]. However, a model with two different structural relaxation mechanisms, is able to account for these experimental findings.

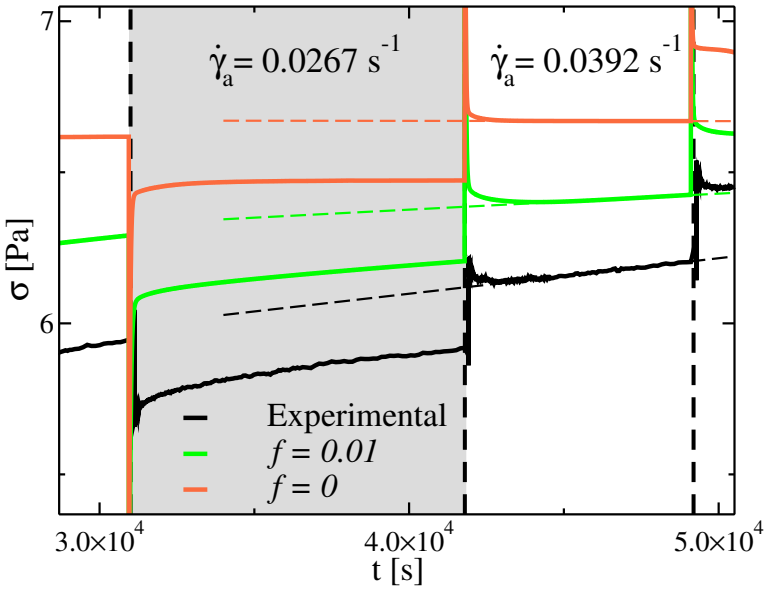

Figure 3.12. Shear stress as a function of time for the last step of the down-sweep and the first step of the up-sweep. Experimental and simulated results for the spatial model are shown for both, one ($f = 0$) and two ($f = 0.01$) time-scale models. The transitions of the shear rate are marked with vertical dotted black lines. The gray background marks the lowest applied shear rate. In the experimental data the slow stress rise after the first shear rate increase is only observed for the model with two time scales. To assist the interpretation, linear fits to the duration to the slow stress rise are shown with dotted lines in the same color as the corresponding simulation/experiment. Publication IV

Hereby the slower relaxation mechanism is causing the slow secondary increase in the stress. This is demonstrated in Fig. 3.12.

3.3.3 Discussion

Some general results can be obtained from Publication IV. In particular it was found that for fluids with non-monotonic flow curves the device geometry (at least for the large gap concentric cylinder geometry) can affect the time evolution which limits the applicability of homogeneous modeling which does not account for these effects. During the up-sweep the model in Publication IV was observed to deviate from the experimental result. In particular during the first few shear rate steps of the up-sweep the stress increased to higher values than in the experiments. In the modeled spatial flow profile the shear rate was observed to be localized close to the rotor during this period. When the high shear rate shear band started to broaden towards the stator, the stress rapidly dropped to a lower value and the successive evolution was again closer to the experimental obser-

vations. Addressing this issue would thus require refining the negative slope and critical shear rate. It is also possible that effects not included in the model, such as elasticity or diffusive terms, might be important for correctly addressing the up-sweep in thixoropic yield stress fluids.

The model in Publication IV was formulated in the terminology of cluster formation. A possible interpretation of the two structural relaxation time scales could be in terms of floc splitting and sizing mechanisms encountered in cellulose suspensions [127, 128]. Spatially resolved flow measurements hint at the existence of clusters or floc structures in the NFC suspensions under flow, despite the high negative charge of NFC fibers [129]. It is also known that the addition of salt heavily affects the rheology of NFC [9]. The origin of the time dependence encountered here and by others [130] requires further research.

Recently, the applicability of the vane geometry for low shear rate measurements of NFC suspensions was questioned [131]. There however, the measurement protocol was very different, no pre-shear was applied and the measurements were started at a low shear rate in contrast to the experiments in Publication III and Publication IV. Further research on this topic is clearly required.

3.4 Wall slip

This section deals with the findings in Publication V which addresses wall slip. Quite often in the flow of complex fluids several phenomena are simultaneously at play. For instance, in experiments transient shear banding is normally accompanied by wall slip [19, 20]. However, even in the absence of any slip, during start-up from a jammed state, a complex fluid could be mistaken to undergo wall slip as the shear localizes very strongly at the rotor. This behavior can be seen in Fig. 3.5. Moreover, different effects can interplay with each other [21, 97]. Thus identifying and understanding the origins of different phenomena is difficult, which makes it complicated to obtain a complete picture of wall slip. The purpose of Publication V was to study a general mechanism which leads to wall slip via a simple model in which complicated convolutions of different effects are absent.

Several origins for wall slip in complex fluids are known. For example for the case of hard spheres, the simple geometrical restriction that particles can not penetrate boundaries, leads to a decreased concentra-

tion close to the wall and thus a lower effective viscosity [132]. For soft deformable particles at high concentrations, on the other hand, the origin of wall slip can be due to a balance between osmotic pressure of the bulk and viscous dissipation [133, 134, 135]. In these known mechanisms the slip occurs at distances from the wall below the scale of one particle diameter. However, for example in diluted emulsions, slip occurred at distances up to tens of orders larger than the droplet diameter [136]. Also in nanocellulose suspensions broad slip layers have been encountered [130]. Large particle free zones have also been encountered in exclusion zones [137, 138]. These exclusion zones are however normally studied without applied shear rate, and can thus not be directly interpreted in terms of wall slip.

3.4.1 Description of the model

The model in Publication V is formulated for the simple system of non-Brownian hard spheres suspended in a Newtonian fluid at volume fractions below jamming. The main consideration is that there is some mechanism which tends to drive the particles away from the wall, while at the same time shear induced particle migration is at play. This will lead to shear rate dependent spatial concentration profiles and thus apparent wall slip, as will be demonstrated shortly. For the particle migration the model by Phillips et al. [88], briefly reviewed in Section 2.4.2, was utilized. Further, in the model the assumption is made that the driving force is counterbalanced by the drag force, and thus the following form for an additional flux term $\mathbf{N_{ex}}$ entering in Eq. (2.14) is obtained

$$\mathbf{N_{ex}} = \phi \frac{\mathbf{F}}{6\pi\eta a}, \tag{3.4}$$

where $\mathbf{F}$ is the force pushing the particle away from the wall, ϕ the volume fraction, and a the particle radius. Here Stokes drag was used and an increase in the drag at higher concentrations is taken into account via the viscosity η, for which the values given by Eq. (2.13) are used.

The model was tested with two different driving potentials: A sedimentation type potential, where $\mathbf{F}$ in Eq. (3.4) is given by

$$\mathbf{F} = \Delta\rho g V_m, \tag{3.5}$$

where $\Delta\rho$ is the density mismatch between the particle and suspending fluid, g the gravitational constant, and V_m the volume of a single particle. This leads to a description which is mostly similar to the one used for

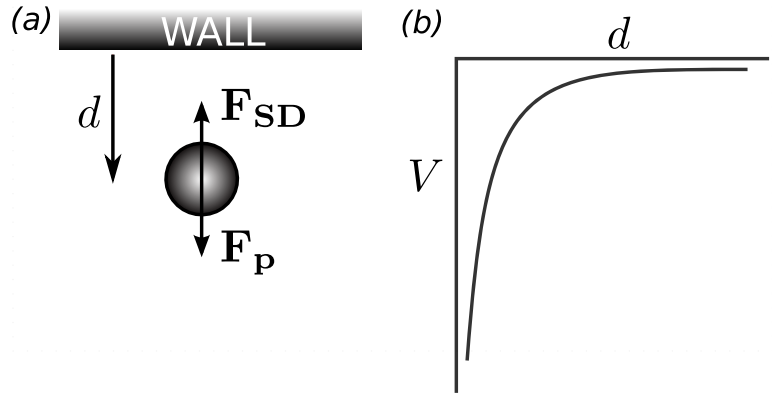

Figure 3.13. (a) A free body diagram of a particle close to the wall and (b) an energy diagram of the repulsive potential. The potential is screened, decaying exponentially. $\mathbf{F}_{\mathrm{SD}}$ denotes the Stokes' drag force and $\mathbf{F}_p$ describes the force due to the repulsive potential. Publication V

studying viscous resuspension in [139]. However, here the focus is different. The intend of the other tested potential was to qualitatively describe particle wall interactions, such as those that could emerge due to entropic reasons, electrostatic forces or ion exchange processes. For this purpose a rather short ranged, decaying Yukawa type potential was chosen. In this case, the repulsive force $\mathbf{F}$ in Eq. (3.4) is given by

$$\mathbf{F} = K_p \frac{e^{-K_s d}}{d^2} + K_p K_s \frac{e^{-K_s d}}{d}, \tag{3.6}$$

where d is the distance from the wall and K_p and K_s are fitting parameters.

These potentials exploit the two extreme cases: the sedimentation potential is constant while the repulsive potential is short ranged with a steep cutoff, resembling to some extent a step function. Thus most real life potentials will lie in between these two. The model is studied by numerically solving for the one dimensional problem of the steady state concentration profile in simple shear between two infinite, parallel plates.

3.4.2 Properties of the model

The qualitative findings of the behavior of the resulting wall slip are for both studied potentials, the sedimentation and the repulsive ones, rather similar. In both cases, the potential tends to drive the particles away from the wall. This results in a lower volume fraction of particles close to the wall i.e. a lubrication layer. The width of these observed lubrication layers depends on the shear rate. This follows readily from the fact that the

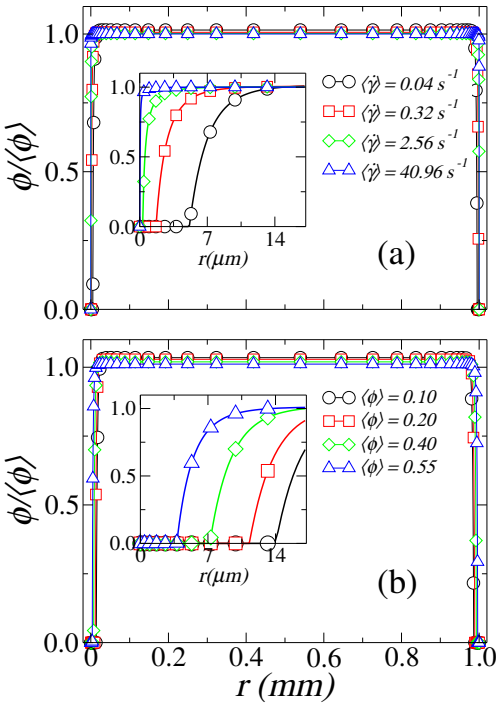

Figure 3.14. (a) Normalized volume fraction and viscosity as a function of distance from the left wall for different shear rates. The average concentration is set to $\langle\phi\rangle = 0.55$. (b) Normalized volume fraction and viscosity as a function of distance from the left wall for different values of $\langle\phi\rangle$. The applied shear rate is $\langle\dot{\gamma}\rangle = 0.32\ (\mathrm{s}^{-1})$. In the insets a close up of the profiles close to the boundary is shown. Publication V

shear induced particle migration scales with the shear rate. The influence of the shear rate on the observed lubrication layer width is shown in Fig. 3.14 a), which depicts the volume fraction as a function of distance from the wall for the repulsive driving potential. In addition to the shear rate, an increase of the average concentration leads also to a decrease of the lubrication layer width. This is demonstrated in Fig. 3.14 b) in the case of the repulsive driving potential.

The differences between the sedimentation and repulsive potential cases are as follows: For the repulsive potential slip occurs at both walls, which is clearly not the case for the sedimentation potential. Further, the short ranged repulsive potential results in a sharp transition from the low concentration close to the wall to the bulk concentration (Fig. 3.14), while for the sedimentation potential the transition is much smoother.

The shear rate dependence of the lubricaton layer leads to more relevant wall slip at low shear rates. In traditional rheometry this would result in mild apparent shear thickening. This behavior is obtained with both

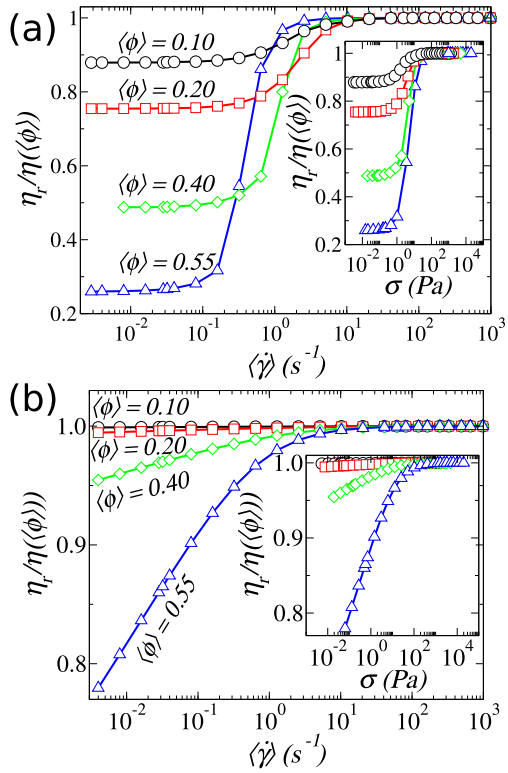

Figure 3.15. The apparent viscosity η_r scaled by the no-slip viscosity as a function of shear rate at different concentrations. The deviations are caused by (a) sedimentation (b) a repulsive potential at the wall, resulting in apparent wall slip. $\eta_r < 1$, that is the apparent viscosity is always smaller than the no-slip result. η_r approaches one with increasing shear rate. The effect is more pronounced at higher concentrations. Insets: Apparent viscosity as a function of the applied stress. Publication V

potentials and should be thus rather independent of the origin of the driving potential. This is demonstrated for both potentials in Fig. 3.15, which shows the rescaled apparent viscosity (unity without slip) as a function of shear rate and as a function of stress (insets).

3.4.3 Discussion

The approach in Publication V can be easily extended by using specific potentials which take into account e.g. the physical chemistry of particle-wall interactions, particle shape dependent configurational restrictions or entropic reasons [140, 138]. This would however require experimental data on the particle volume fraction. Also addressing the time evolution, would benefit from detailed experiments, and requires model development [96]. Similarly addressing the generality of the wall slip mechanism

beyond hard, spherical particles, requires further research especially in what comes to the particle migration mechanism.

4. Summary

In this thesis the rheology of complex fluids was addressed using continuum models. In the utilized models the shear stress is purely viscous with the viscosity being a function of the structure, in particular the volume fraction. Particular emphasis was given on the emergence of spatial effects in flows with time dependent structure evolution. This was realized by making spatially resolved simulations in addition to those in homogeneous laminar shear flow. In particular, the one dimensional spatial resolution was mainly realized in the radial direction of the concentric cylinder Couette geometry, allowing for qualitative comparison with relevant experimental results.

In Publication I a model for aggregating colloidal suspensions, based on population balance equations, was studied in the light of yield stress fluids. The focus laid on the start-up transient behavior and the steady state. In Publication II a structural model was utilized for studying shear rate sweeps for simple time-dependent yield stress fluids. Publication III and IV dealt with practical issues arising when dealing with the rheology of nanocellulose suspensions. In particular Publication III dealt with steady state flow curve measurements, while in Publication IV also the time evolution was addressed via modeling. There spatially resolved shear rate sweeps employing a structural model for thixotropic yield stress fluids were compared to the corresponding experimental results. Publication V addressed wall slip with a simple model based on the interplay between shear induced particle migration and external driving potentials.

The fact that the models in this thesis are continuum scale ones results obviously in certain restrictions. Discrete models are required to shed light on these aspects. Another task which requires further work and the combination of experiments and theory is to establish a better connection between the fluid properties and the rheological behavior, such as for ex-

ample the ion concentration in NFC suspensions [9]. This would allow for the development of predictive models, which would be very useful in the design and development of new applications.

Several experimentally relevant phenomena are currently left out from the models. For the models utilized in this thesis, the stress was purely viscous, and elastic effects were mostly neglected (except for Publication II). Also the development of models for wall slip in yield stress fluids and their subsequent coupling to fluid models still requires a lot of work. Further, it was found that for addressing shear rate ramps in thixotropic yield stress fluids, the inclusion of additional effects might be important.

A question which remains to be resolved is to which extend the steady state flow curve and the transient behavior in yield stress fluids are connected [20]. The coupling was addressed in Publication I, but no definite results on this topic could be obtained with the used model. In the structural models, as explicitly demonstrated in Publication IV, the time evolution can be scaled without affecting the steady state flow curve.

The model in Publication I exhibits a unique static yield stress for a sufficiently jammed initial state. On the other hand, in stress startup experiments of thixotropic yield stress fluids, the initial state is often obtained through pre-shear and a subsequent rest period. In the static yield stress measurements of Publication IV, the jammed initial state was obtained through the application of a low stress for a fixed time. However, it was not studied whether the static yield stress was unique with respect to the stress used in the initialization. Very different behavior was recently observed in carbon black suspensions, where the yield stress could be quite arbitrarily tuned, through the application of a stress prior to the experiment [141].

Bibliography

[1] R. Edgeworth, B.J. Dalton, and T. Parnell. The pitch drop experiment. *Eur. J. Phys.*, 5(4):198–200, 1984.

[2] P.F.G. Banfill. Rheology of fresh cement and concrete. *Rheology reviews*, 2006:61–130, 2006.

[3] R. Mendes, G. Vinay, G. Ovarlez, and P. Coussot. Modeling the rheological behavior of waxy crude oils as a function of flow and temperature history. *J. Rheol.*, 59(3):703–732, 2015.

[4] I. Siró and D. Plackett. Microfibrillated cellulose and new nanocomposite materials: a review. *Cellulose*, 17(3):459–494, 2010.

[5] D. Ishii, T. Saito, and A. Isogai. Viscoelastic evaluation of average length of cellulose nanofibers prepared by TEMPO-mediated oxidation. *Biomacromolecules*, 12(3):548–550, 2011.

[6] A.B. Fall, S.B. Lindström, O. Sundman, L. Ödberg, and L. Wågberg. Colloidal stability of aqueous nanofibrillated cellulose dispersions. *Langmuir*, 27(18):11332–11338, 2011.

[7] M. Iotti, Ø.W. Gregersen, S. Moe, and M. Lenes. Rheological studies of microfibrillar cellulose water dispersions. *J. Polym. Environ.*, 19(1):137–145, 2011.

[8] E. Saarikoski, T. Saarinen, J. Salmela, and J. Seppälä. Flocculated flow of microfibrillated cellulose water suspensions: an imaging approach for characterisation of rheological behaviour. *Cellulose*, 19(3):647–659, 2012.

[9] H. Fukuzumi, R. Tanaka, T. Saito, and A. Isogai. Dispersion stability and aggregation behavior of TEMPO-oxidized cellulose nanofibrils in water as a function of salt addition. *Cellulose*, 21(3):1553–1559, 2014.

[10] J. Mewis. Thixotropy-a general review. *J. Non-Newton. Fluid Mech.*, 6(1):1–20, 1979.

[11] H.A. Barnes. Thixotropy—a review. *J. Non-Newton. Fluid Mech.*, 70(1):1–33, 1997.

[12] J. Mewis and N.J. Wagner. Thixotropy. *Adv. Colloid Interface Sci.*, 147–148:214–227, 2009.

[13] H.A. Barnes. The yield stress—a review or '$\pi\alpha\nu\tau\alpha\ \rho\varepsilon\iota$'—everything flows? *J. Non-Newton. Fluid Mech.*, 81(1):133–178, 1999.

[14] P.C.F. Møller, A. Fall, and D. Bonn. Origin of apparent viscosity in yield stress fluids below yielding. *EPL*, 87(3):38004, 2009.

[15] Q.D. Nguyen and D.V. Boger. Measuring the flow properties of yield stress fluids. *Annu. Rev. Fluid Mech.*, 24(1):47–88, 1992.

[16] P. Coussot, Q.D. Nguyen, H.T. Huynh, and D. Bonn. Avalanche behavior in yield stress fluids. *Phys. Rev. Lett.*, 88(17):175501, 2002.

[17] P.C.F. Møller, J. Mewis, and D. Bonn. Yield stress and thixotropy: on the difficulty of measuring yield stresses in practice. *Soft Matter*, 2(4):274–283, 2006.

[18] P.C.F. Møller, S. Rodts, M.A.J. Michels, and D. Bonn. Shear banding and yield stress in soft glassy materials. *Phys. Rev. E*, 77(4):041507, 2008.

[19] T. Divoux, D. Tamarii, C. Barentin, and S. Manneville. Transient shear banding in a simple yield stress fluid. *Phys. Rev. Lett.*, 104(20):208301, 2010.

[20] T. Divoux, C. Barentin, and S. Manneville. From stress-induced fluidization process to Herschel-Bulkley behaviour in simple yield stress fluids. *Soft Matter*, 7(18):8409–8418, 2011.

[21] R. Buscall. Letter to the Editor: Wall slip in dispersion rheometry. *J. Rheol.*, 54(6):1177–1183, 2010.

[22] P. Coussot. Yield stress fluid flows: A review of experimental data. *J. Non-Newton. Fluid Mech.*, 211:31–49, 2014.

[23] D. Bonn, J. Paredes, M. M Denn, L. Berthier, T. Divoux, and S. Manneville. Yield stress materials in soft condensed matter. *arXiv preprint arXiv:1502.05281*, 2015.

[24] Faith A Morrison. *Understanding rheology*. Oxford University Press, 2001.

[25] H.F. George and F. Qureshi. Newton's Law of Viscosity, Newtonian and Non-Newtonian Fluids. In *Encyclopedia of Tribology*, pages 2416–2420. Springer US, 2013.

[26] E. Brown and H.M. Jaeger. Shear thickening in concentrated suspensions: phenomenology, mechanisms and relations to jamming. *Rep. Prog. Phys.*, 77(4):046602, 2014.

[27] J. Bleyer, M. Maillard, P. De Buhan, and P. Coussot. Efficient numerical computations of yield stress fluid flows using second-order cone programming. *Comput. Method. Appl. M.*, 283:599–614, 2015.

[28] D. Bonn and M.M. Denn. Yield stress fluids slowly yield to analysis. *Science*, 324(5933):1401–1402, 2009.

[29] A.J. Liu and S.R. Nagel. Nonlinear dynamics: Jamming is not just cool any more. *Nature*, 396(6706):21–22, 1998.

[30] V. Trappe, V. Prasad, L. Cipelletti, P.N. Segre, and D.A. Weitz. Jamming phase diagram for attractive particles. *Nature*, 411(6839):772–775, 2001.

[31] S.M. Fielding. Shear banding in soft glassy materials. *Rep. Prog. Phys.*, 77(10):102601, 2014.

[32] T. Divoux, V. Grenard, and S. Manneville. Rheological hysteresis in soft glassy materials. *Phys. Rev. Lett.*, 110(1):018304, 2013.

[33] D. Vlassopoulos and M. Cloitre. Tunable rheology of dense soft deformable colloids. *Curr. Opin. Colloid Interface Sci.*, 19(6):561–574, 2014.

[34] T. Voigtmann. Nonlinear glassy rheology. *Curr. Opin. Colloid Interface Sci.*, 19(6):549–560, 2014.

[35] G. Petekidis, D. Vlassopoulos, and P.N. Pusey. Yielding and flow of sheared colloidal glasses. *J. Phys. Condens. Matter*, 16(38):S3955–S3963, 2004.

[36] H.M. Shewan and J.R. Stokes. Analytically predicting the viscosity of hard sphere suspensions from the particle size distribution. *J. Non-Newton. Fluid Mech.*, DOI:10.1016/j.jnnfm.2014.09.002, 2014.

[37] J. Paredes, M.A.J. Michels, and D. Bonn. Rheology across the zero-temperature jamming transition. *Phys. Rev. Lett.*, 111(1):015701, 2013.

[38] E. Irani, P. Chaudhuri, and C. Heussinger. Impact of attractive interactions on the rheology of dense athermal particles. *Phys. Rev. Lett.*, 112(18):188303, 2014.

[39] A. Kurokawa, V. Vidal, K. Kurita, T. Divoux, and S. Manneville. Avalanche-like fluidization of an attractive dispersion. *arXiv preprint arXiv:1505.06137*, 2015.

[40] G.B. Jeffery. The motion of ellipsoidal particles immersed in a viscous fluid. *P. R. Soc. Lond. A-Conta.*, 102(715):161–179, 1922.

[41] F. Folgar and C.L. Tucker. Orientation behavior of fibers in concentrated suspensions. *J. Reinf. Plast. Comp.*, 3(2):98–119, 1984.

[42] P. Kumar, D. Gold, D.L. Blair, A. Baskaran, and J.S. Urbach. Shear-driven aggregation of SU-8 microrods in suspension. *Soft Matter*, 10(34):6514–6519, 2014.

[43] A. Puisto, X. Illa, M. Mohtaschemi, and M.J. Alava. Modeling the viscosity and aggregation of suspensions of highly anisotropic nanoparticles. *Eur. Phys. J. E*, 35(1):1–7, 2012.

[44] W.K.A. Ma, F. Chinesta, A. Ammar, and M.R. Mackley. Rheological modeling of carbon nanotube aggregate suspensions. *J. Rheol.*, 52(6):1311–1330, 2008.

[45] O. Eriksen, K. Syverud, and O. Gregersen. The use of microfibrillated cellulose produced from kraft pulp as strength enhancer in tmp paper. *Nord. Pulp Paper Res. J.*, 23(3):299–304, 2008.

[46] Y. Okahisa, A. Yoshida, S. Miyaguchi, and H. Yano. Optically transparent wood–cellulose nanocomposite as a base substrate for flexible organic light-emitting diode displays. *Compos. Sci. Technol.*, 69(11):1958–1961, 2009.

[47] S.J. Eichhorn, A. Dufresne, M. Aranguren, N.E. Marcovich, J.R. Capadona, S.J. Rowan, C. Weder, W. Thielemans, M. Roman, S. Renneckar, W. Gindl, S. Veigel, J. Keckes, H. Yano, K. Abe, M. Nogi, A.N. Nakagaito,

A. Mangalam, J. Simonsen, A.S. Benight, A. Bismarck, L.A. Berglund, and T. Peijs. Review: current international research into cellulose nanofibres and nanocomposites. *J. Mater. Sci.*, 45(1):1–33, 2010.

[48] A.F. Turbak, F.W. Snyder, and K.R. Sandberg. Microfibrillated cellulose, a new cellulose product: Properties, uses and commercial potential. *J. Appl. Polym. Sci.: Appl. Poly. Symp.*, 37:815–827, 1983.

[49] HPS Abdul Khalil, AH Bhat, A Abu Bakar, Paridah Md Tahir, ISM Zaidul, and M Jawaid. Cellulosic nanocomposites from natural fibers for medical applications: A review. In *Handbook of Polymer Nanocomposites. Processing, Performance and Application*, pages 475–511. Springer, 2015.

[50] M.A. Hubbe, O.J. Rojas, L.A. Lucia, and M. Sain. Cellulosic nanocomposites: a review. *BioResources*, 3(3):929–980, 2008.

[51] J. Araki. Electrostatic or steric?–preparations and characterizations of well-dispersed systems containing rod-like nanowhiskers of crystalline polysaccharides. *Soft Matter*, 9(16):4125–4141, 2013.

[52] M. Bercea and P. Navard. Shear dynamics of aqueous suspensions of cellulose whiskers. *Macromolecules*, 33(16):6011–6016, 2000.

[53] M.A.S. Azizi Samir, F. Alloin, and A. Dufresne. Review of recent research into cellulosic whiskers, their properties and their application in nanocomposite field. *Biomacromolecules*, 6(2):612–626, 2005.

[54] F.W. Herrick, R.L. Casebier, J.K. Hamilton, and K.R. Sandberg. Microfibrillated cellulose: morphology and accessibility. In *J. Appl. Polym. Sci.: Appl. Polym. Symp.;(United States)*, volume 37, pages CONF–8205234–Vol. 2. ITT Rayonier Inc., Shelton, WA, 1983.

[55] M. Pääkkö, M. Ankerfors, H. Kosonen, A. Nykänen, S. Ahola, M. Österberg, J. Ruokolainen, J. Laine, P.T. Larsson, O. Ikkala, and T. Lindström. Enzymatic hydrolysis combined with mechanical shearing and high-pressure homogenization for nanoscale cellulose fibrils and strong gels. *Biomacromolecules*, 8(6):1934–1941, 2007.

[56] T. Saito, Y. Nishiyama, J.-L. Putaux, M. Vignon, and A. Isogai. Homogeneous suspensions of individualized microfibrils from TEMPO-catalyzed oxidation of native cellulose. *Biomacromolecules*, 7(6):1687–1691, 2006.

[57] T. Saito, S. Kimura, Y. Nishiyama, and A. Isogai. Cellulose nanofibers prepared by TEMPO-mediated oxidation of native cellulose. *Biomacromolecules*, 8(8):2485–2491, 2007.

[58] A. Isogai, T. Saito, and H. Fukuzumi. TEMPO-oxidized cellulose nanofibers. *Nanoscale*, 3(1):71–85, 2011.

[59] E. Lasseuguette, D. Roux, and Y. Nishiyama. Rheological properties of microfibrillar suspension of TEMPO-oxidized pulp. *Cellulose*, 15(3):425–433, 2008.

[60] M.-P. Lowys, J. Desbrieres, and M. Rinaudo. Rheological characterization of cellulosic microfibril suspensions. role of polymeric additives. *Food Hydrocolloids*, 15(1):25–32, 2001.

[61] B. Derakhshandeh, R.J. Kerekes, S.G. Hatzikiriakos, and C.P.J. Bennington. Rheology of pulp fibre suspensions: A critical review. *Chem. Eng. Sci.*, 66(15):3460–3470, 2011.

[62] R.J. Kerekes, R.M. Soszynski, and T. Doo. The flocculation of pulp fibres. In *Papermaking Raw Materials: Their Interaction with the Production Process and Their Effect on Paper Properties-Transactions of the Eighth Fundamental Research Symposium held at Oxford: September 1985*, pages 265–310. Mechanical Engineering Publications Limited, 1985.

[63] D.M. Martinez, K. Buckley, S. Jivan, A. Lindstrom, R. Thiruvengadaswamy, J.A. Olson, T.J. Ruth, and R.J. Kerekes. Characterizing the mobility of papermaking fibres during sedimentation. In *The science of papermaking: transactions of the 12th fundamental research symposium, Oxford. The Pulp and Paper Fundamental Research Society, Bury, UK*, pages 225–254, 2001.

[64] A. Celzard, V. Fierro, and R. Kerekes. Flocculation of cellulose fibres: new comparison of crowding factor with percolation and effective-medium theories. *Cellulose*, 16(6):983–987, 2009.

[65] M.B. Liu and G.R. Liu. Smoothed particle hydrodynamics (sph): an overview and recent developments. *Archives of computational methods in engineering*, 17(1):25–76, 2010.

[66] J. Hämäläinen, S.B. Lindström, T. Hämäläinen, and H. Niskanen. Papermaking fibre-suspension flow simulations at multiple scales. *Journal of Engineering Mathematics*, 71(1):55–79, 2011.

[67] S.B. Lindström and T. Uesaka. A numerical investigation of the rheology of sheared fiber suspensions. *Physics of Fluids (1994-present)*, 21(8):083301, 2009.

[68] H. Niskanen, H. Eloranta, J. Tuomela, and J. Hämäläinen. On the orientation probability distribution of flexible fibres in a contracting channel flow. *International Journal of Multiphase Flow*, 37(4):336–345, 2011.

[69] T. Hamalainen and J. Hamalainen. Fibre floc evolution model, part i: flocculation in a headbox. *Nordic Pulp & Paper Research Journal*, 25(1):39–47, 2010.

[70] T. Hamalainen and J. Hamalainen. Fibre floc evolution model, part ii: Influence of jet-to-wire ratio on the resulting fibre floc evolution in the initial drainage zone. *NORDIC PULP & PAPER RESEARCH JOURNAL*, 25(1):48–55, 2010.

[71] P.J. Krochak, J.A. Olson, and D.M. Martinez. Fiber suspension flow in a tapered channel: the effect of flow/fiber coupling. *International Journal of Multiphase Flow*, 35(7):676–688, 2009.

[72] B. Derakhshandeh, S.G. Hatzikiriakos, and C.P.J. Bennington. Rheology of pulp suspensions using ultrasonic doppler velocimetry. *Rheologica acta*, 49(11-12):1127–1140, 2010.

[73] B. Derakhshandeh. *Rheology of low to medium consistency pulp fibre suspensions (Doctoral dissertation)*. PhD thesis, University of British Columbia (Vancouver, 2011.

[74] B. Derakhshandeh, D. Vlassopoulos, and S.G. Hatzikiriakos. Thixotropy, yielding and ultrasonic doppler velocimetry in pulp fibre suspensions. *Rheologica acta*, 51(3):201–214, 2012.

[75] J. Hämäläinen, R. Eskola, A.-L. Erkkilä, and T. Leppänen. Rheology in papermaking—from fibre suspension flows to mechanics of solid paper. *Korea-Australia Rheology Journal*, 23(4):211–217, 2011.

[76] A.I.A. Malkin, A.Y. Malkin, and A.I. Isayev. *Rheology: concepts, methods & applications*. Chem Tec Pub, 2006.

[77] P. Coussot. *Rheometry of pastes, suspensions, and granular materials: applications in industry and environment*. Wiley-Interscience, 2005.

[78] K. Hyun, M. Wilhelm, C.O. Klein, K.S. Cho, J.G. Nam, K.H. Ahn, S.J. Lee, R.H. Ewoldt, and G.H. McKinley. A review of nonlinear oscillatory shear tests: Analysis and application of large amplitude oscillatory shear (LAOS). *Prog. Polym. Sci*, 36(12):1697–1753, 2011.

[79] J.M. Simmons. A servo-controlled rheometer for measurement of the dynamic modulus of viscoelastic liquids. *J. Sci. Instrum.*, 43(12):887, 1966.

[80] R.I. Tanner and J.M. Simmons. Combined simple and sinusoidal shearing in elastic liquids. *Chem. Eng. Sci.*, 22(12):1803–1815, 1967.

[81] J. Vermant, P. Moldenaers, J. Mewis, M. Ellis, and R. Garritano. Orthogonal superposition measurements using a rheometer equipped with a force rebalanced transducer. *Rev. Sci. Instrum.*, 68(11):4090–4096, 1997.

[82] S. Kim, J. Mewis, C. Clasen, and J. Vermant. Superposition rheometry of a wormlike micellar fluid. *Rheol. Acta*, 52(8-9):727–740, 2013.

[83] S. Manneville, L. Bécu, and A. Colin. High-frequency ultrasonic speckle velocimetry in sheared complex fluids. *Eur. Phys. J. Appl. Phys.*, 28(03):361–373, 2004.

[84] S. Haavisto, A.I. Koponen, and J. Salmela. New insight into rheology and flow properties of complex fluids with doppler optical coherence tomography. *Front. Chem.*, 2:27, 2014.

[85] C.J. Elkins and M.T. Alley. Magnetic resonance velocimetry: applications of magnetic resonance imaging in the measurement of fluid motion. *Exp. Fluids*, 43(6):823–858, 2007.

[86] P.D. Olmsted. Perspectives on shear banding in complex fluids. *Rheol. Acta*, 47(3):283–300, 2008.

[87] P. Coussot and G. Ovarlez. Physical origin of shear-banding in jammed systems. *Eur. Phys. J. E*, 33(3):183–188, 2010.

[88] R.J. Phillips, R.C. Armstrong, R.A. Brown, A.L. Graham, and J.R. Abbott. A constitutive equation for concentrated suspensions that accounts for shear induced particle migration. *Phys. Fluids A*, 4(1):30–40, 1992.

[89] A. Einstein. Eine neue Bestimmung der Moleküldimensionen. *Annalen der Physik*, 324(2):289–306, 1906.

[90] A. Einstein. Berichtigung zu meiner Arbeit:„Eine neue Bestimmung der Moleküldimensionen". *Annalen der Physik*, 339(3):591–592, 1911.

[91] G.K. Batchelor. The effect of Brownian motion on the bulk stress in a suspension of spherical particles. *J. Fluid Mech.*, 83(01):97–117, 1977.

[92] A.V. Shenoy. *Rheology of filled polymer systems*. Springer Science & Business Media, 1999.

[93] I.M. Krieger and T.J. Dougherty. A mechanism for non-Newtonian flow in suspensions of rigid spheres. *Trans. Soc. Rheol.*, 3(1):137–152, 1959.

[94] S.H. Maron and P.E. Pierce. Application of ree-eyring generalized flow theory to suspensions of spherical particles. *J. Colloid Sci.*, 11(1):80–95, 1956.

[95] D. Quemada. Rheology of concentrated disperse systems and minimum energy dissipation principle. *Rheol. Acta*, 16(1):82–94, 1977.

[96] M.S. Ingber, A.L. Graham, L.A. Mondy, and Z. Fang. An improved constitutive model for concentrated suspensions accounting for shear-induced particle migration rate dependence on particle radius. *Int. J. Multiphase Flow*, 35(3):270–276, 2009.

[97] T. Gibaud, D. Frelat, and S. Manneville. Heterogeneous yielding dynamics in a colloidal gel. *Soft Matter*, 6(15):3482–3488, 2010.

[98] D. Ramkrishna. *Population balances: Theory and applications to particulate systems in engineering*. Academic press, 2000.

[99] V. Runkana, P. Somasundaran, and P.C. Kapur. Mathematical modeling of polymer-induced flocculation by charge neutralization. *J. Colloid Interface Sci.*, 270(2):347–358, 2004.

[100] V. Runkana, P. Somasundaran, and P.C. Kapur. A population balance model for flocculation of colloidal suspensions by polymer bridging. *Chem. Eng. Sci.*, 61(1):182–191, 2006.

[101] M. von Smoluchowski. Versuch einer mathematischen Theorie der Koagulationskinetik kolloider Lösungen. *Z. phys. Chem*, 92:129–168, 1917.

[102] P.L. Krapivsky, S. Redner, and E. Ben-Naim. *A kinetic view of statistical physics*. Cambridge University Press, 2010.

[103] D. Ramkrishna and M.R. Singh. Population balance modeling: Current status and future prospects. *Annu. Rev. Chem. Biomol. Eng.*, 5:123–146, 2014.

[104] M.U. Bäbler. A collision efficiency model for flow induced coagulation of fractal aggregates. *AIChE J.*, 54:1748–1760, 2008.

[105] D.L. Swift and S.K. Friedlander. The coagulation of hydrosols by Brownian motion and laminar shear flow. *J. Colloid Sci.*, 19(7):621–647, 1964.

[106] M.U. Bäbler and M. Morbidelli. Analysis of the aggregation–fragmentation population balance equation with application to coagulation. *J. Colloid Interface Sci.*, 316(2):428–441, 2007.

[107] M. Soos, J. Sefcik, and M. Morbidelli. Investigation of aggregation, breakage and restructuring kinetics of colloidal dispersions in turbulent flows by population balance modeling and static light scattering. *Chem. Eng. Sci.*, 61(8):2349–2363, 2006.

[108] P.T. Spicer and S.E. Pratsinis. Coagulation and fragmentation: Universal steady-state particle-size distribution. *AIChE J.*, 42(6):1612–1620, 1996.

[109] A. Mujumdar, A.N. Beris, and A.B. Metzner. Transient phenomena in thixotropic systems. *J. Non-Newton. Fluid Mech.*, 102(2):157–178, 2002.

[110] X. Illa, A. Puisto, A. Lehtinen, M. Mohtaschemi, and M.J. Alava. Transient shear banding in time-dependent fluids. *Phys. Rev. E*, 87(2):022307, 2013.

[111] P. Sollich, F. Lequeux, P. Hébraud, and M.E. Cates. Rheology of soft glassy materials. *Phys. Rev. Lett.*, 78(10):2020–2023, Mar 1997.

[112] J.S. Langer. Dynamics of shear-transformation zones in amorphous plasticity: Formulation in terms of an effective disorder temperature. *Phys. Rev. E*, 70(4):041502, 2004.

[113] P. Chaudhuri, L. Berthier, and L. Bocquet. Inhomogeneous shear flows in soft jammed materials with tunable attractive forces. *Phys. Rev. E*, 85(2):021503, 2012.

[114] S.M. Fielding, M.E. Cates, and P. Sollich. Shear banding, aging and noise dynamics in soft glassy materials. *Soft Matter*, 5(12):2378–2382, 2009.

[115] R.L. Moorcroft, M.E. Cates, and S.M. Fielding. Age-dependent transient shear banding in soft glasses. *Phys. Rev. Lett.*, 106(5):055502, 2011.

[116] A.R. Hinkle and M.L. Falk. A rate-dependent effective-temperature model of shear band formation during flow. *arXiv preprint arXiv:1502.01291*, 2015.

[117] A. Lehtinen, A. Puisto, X. Illa, M. Mohtaschemi, and M.J. Alava. Transient shear banding in viscoelastic Maxwell fluids. *Soft Matter*, 9(33):8041–8049, 2013.

[118] R. Folkersma, A.J.G. van Diemen, J. Laven, and H.N. Stein. Steady shear rheology of dilute polystyrene particle gels. *Rheol. Acta*, 38(4):257–267, 1999.

[119] A. Ragouilliaux, G. Ovarlez, N. Shahidzadeh-Bonn, B. Herzhaft, T. Palermo, and P. Coussot. Transition from a simple yield-stress fluid to a thixotropic material. *Phys. Rev. E*, 76(5):051408, 2007.

[120] T. Saarinen, S. Haavisto, A. Sorvari, J. Salmela, and J. Seppälä. The effect of wall depletion on the rheology of microfibrillated cellulose water suspensions by optical coherence tomography. *Cellulose*, 21(3):1261–1275, 2014.

[121] G. Ovarlez, S. Rodts, A. Ragouilliaux, P. Coussot, J. Goyon, and A. Colin. Wide-gap Couette flows of dense emulsions: Local concentration measurements, and comparison between macroscopic and local constitutive law measurements through magnetic resonance imaging. *Phys. Rev. E*, 78(3):036307, 2008.

[122] D.T. Fisher, S.A. Clayton, D.V. Boger, and P.J. Scales. The bucket rheometer for shear stress-shear rate measurement of industrial suspensions. *J. Rheol.*, 51(5):821–831, 2007.

[123] A. Sneck. New approach to classification of cellulose fibrils and suitable methods for their characterization. In *TAPPI International conference on nanotechnology for renewable materials, June*, pages 6–8, 2011.

[124] H.A. Barnes and J.O. Carnali. The vane-in-cup as a novel rheometer geometry for shear thinning and thixotropic materials. *J. Rheol.*, 34(6):841–866, 1990.

[125] J. Goyon, A. Colin, G. Ovarlez, A. Ajdari, and L. Bocquet. Spatial cooperativity in soft glassy flows. *Nature*, 454(7200):84–87, 2008.

[126] I.M. Krieger and S.H. Maron. Direct determination of the flow curves of non-Newtonian fluids. *J. Appl. Phys.*, 23(1):147–149, 1952.

[127] U. Bjorkman. The metarheology of crowded fibre suspensions. *Ann. T. Nord. Rheol. Soc*, 14:69, 2006.

[128] U. Björkman. Floc dynamics in flowing fibre suspensions. *Nord. Pulp Paper Res. J.*, 20(2):247–252, 2005.

[129] A. Karppinen. Rheology and flocculation of polymer-modified microfibrillated cellulose suspensions (Doctoral dissertation). *Aalto University*, 2014.

[130] F. Martoïa, C. Perge, P.J.J. Dumont, L. Orgéas, M. Fardin, S. Manneville, and M.N. Belgacem. Heterogeneous flow kinematics of cellulose nanofibril suspensions under shear. *Soft Matter*, DOI:10.1039/C5SM00530B, 2015.

[131] O. Nechyporchuk, M.N. Belgacem, and F. Pignon. Concentration effect of TEMPO-oxidized nanofibrillated cellulose aqueous suspensions on the flow instabilities and small-angle X-ray scattering structural characterization. *Cellulose*, DOI:10.1007/s10570-015-0640-0, 2015.

[132] S.C. Jana, B. Kapoor, and A. Acrivos. Apparent wall slip velocity coefficients in concentrated suspensions of noncolloidal particles. *J. Rheol.*, 39(6):1123–1132, 1995.

[133] S.P. Meeker, R.T. Bonnecaze, and M. Cloitre. Slip and flow in soft particle pastes. *Phys. Rev. Lett.*, 92(19):198302, 2004.

[134] S.P. Meeker, R.T. Bonnecaze, and M. Cloitre. Slip and flow in soft particles: Direct observation and rheology. *J. Rheol.*, 48(6):1295–1320, 2004.

[135] J.R. Seth, M. Cloitre, and R.T. Bonnecaze. Influence of short-range forces on wall-slip in microgel pastes. *J. Rheol.*, 52(5):1241–1268, 2008.

[136] J.-B. Salmon, L. Bécu, S. Manneville, and A. Colin. Towards local rheology of emulsions under Couette flow using dynamic light scattering. *Eur. Phys. J. E*, 10(3):209–221, 2003.

[137] J. Zheng, W.-C. Chin, E. Khijniak, E.J. Khijniak, and G.H. Pollack. Surfaces and interfacial water: evidence that hydrophilic surfaces have long-range impact. *Adv. Colloid Interface Sci.*, 127(1):19–27, 2006.

[138] D. Florea, S. Musa, J.M.R. Huyghe, and H.M. Wyss. Long-range repulsion of colloids driven by ion exchange and diffusiophoresis. *Proc. Natl. Acad. Sci.*, 111(18):6554–6559, 2014.

[139] D. Leighton and A. Acrivos. Viscous resuspension. *Chem. Eng. Sci.*, 41(6):1377–1384, 1986.

[140] J. Sanchez-Reyes and L.A. Archer. Interfacial slip violations in polymer solutions: Role of microscale surface roughness. *Langmuir*, 19(8):3304–3312, 2003.

[141] G. Ovarlez, L. Tocquer, F. Bertrand, and P. Coussot. Rheopexy and tunable yield stress of carbon black suspensions. *Soft Matter*, 9(23):5540–5549, 2013.

Aalto-DD 152/2015

ISBN 978-952-60-6419-2 (printed)
ISBN 978-952-60-6420-8 (pdf)
ISSN-L 1799-4934
ISSN 1799-4934 (printed)
ISSN 1799-4942 (pdf)

Aalto University
School of Science
Department of Applied Physics
www.aalto.fi

BUSINESS + ECONOMY

ART + DESIGN + ARCHITECTURE

SCIENCE + TECHNOLOGY

CROSSOVER

DOCTORAL DISSERTATIONS